

## Mudstone diagenesis and sandstone provenance in an Upper Jurassic – Lower Cretaceous evolving half-graben system, Wollaston Forland, North-East Greenland

Mette Olivarius<sup>1</sup>, Afsoon M. Kazerouni<sup>2</sup>, Rikke Weibel<sup>1</sup>, Thomas F. Kokfelt<sup>3</sup>, Jussi Hovikoski<sup>4,5</sup>

<sup>1</sup>Department for Geo-energy and Storage, Geological Survey of Denmark and Greenland (GEUS), Copenhagen, Denmark; <sup>2</sup>Geological Survey of Denmark and Greenland (GEUS), Copenhagen, Denmark; <sup>3</sup>Department for Mapping and Mineral Resources, Geological Survey of Denmark and Greenland (GEUS), Copenhagen, Denmark; <sup>4</sup>Department for Geophysics and Sedimentary Basins, Geological Survey of Denmark and Greenland (GEUS), Copenhagen, Denmark; <sup>5</sup>Geological Survey of Finland (GTK), Espoo, Finland

### Abstract

The influence of rifting on the composition of Kimmeridgian to Barremian mudstones from northern Wollaston Forland, North-East Greenland is investigated by petrographic and mineralogical analyses of the Brorson Halvø-1 and Rødryggen-1 cores, and provenance analysis by zircon U-Pb age dating of nearby sandstones. Mudstone composition varies systematically as a function of the timing of rifting progression and position in the half-graben depositional system. Pyrite primarily precipitated in the early rift to rift climax phases. Euhedral pyrite overgrowths on framboids formed only during the rift climax phase (Lindemans Bugt Formation). Dolomite is the dominant carbonate cement, except for the sediments deposited in the early waning rift phase (Palnatokes Bjerg Formation) where calcite is dominant, and in the late waning rift phase (Stratumbjerg Formation) where siderite dominates. The highest-temperature reactions with precipitation of illite, quartz, ankerite and barite signify sediment burial depths of >2 km prior to exhumation. Uplift-induced fracturing occurred mainly in the early rift to rift acceleration succession (Bernbjerg Formation). Mudstones in the proximal part of the half-graben (Rødryggen-1) include more detrital kaolinite than the distal mudstones (Brorson Halvø-1), which contain more mixed-layer illite-smectite and illite. Vermiculite was deposited only in the proximal part of the basin in the rift climax and waning rift successions. Chlorite was deposited proximally and distally during the waning rift phase, though supply began earlier in the distal part. Fine-grained sediment in the distal part of the half-graben was therefore probably supplied by axial transport from Palaeoproterozoic crystalline rocks and Meso- to Neoproterozoic metamorphic rocks located to the north and north-west. This agrees with the zircon provenance signature from outcropping sand-rich facies, where zircon grains with U-Pb ages of 2.0–1.6 Ga are dominant, in addition to common 1.6–0.9 Ga ages, and fewer 2.8–2.6 Ga and 0.47–0.36 Ga ages.

### 1. Introduction

The archetypal half-graben setting has an ample sediment supply and can be divided into several sedimentation zones related to proximity to bounding faults and rift evolution (Surlyk 1978; Gawthorpe & Leeder 2000). This subdivision contributes to evaluations of sediment distribution in basins. Moreover, when knowledge of structural evolution is combined with information on basement rocks in a hinterland area and sediment delivery systems, changes in sediment composition can be linked to source changes over time.

Possible trends in sediment composition are not well-known in distal marine half-grabens that may be largely isolated from coarse-grained clastic input by coast-parallel submarine rift shoulders. Such a setting results in axial sediment transport and mudstone deposition, particularly in basins detached from the coastal area. Therefore, the Rødryggen-1 and Brorson Halvø-1 cores from northern Wollaston Forland in North-East Greenland (Fig. 1) were used in this study to investigate the proximal versus distal development of a mudstone-dominated half-graben succession deposited during Late Jurassic to Early Cretaceous rifting. Organic-rich black shales

**\*Correspondence:** [mol@geus.dk](mailto:mol@geus.dk)

**Received:** 03 Jan 2022

**Revised:** 03 Oct 2023

**Accepted:** 03 Oct 2023

**Published:** 21 Dec 2023

**Keywords:** diagenetic processes, mudstone mineralogy, petrography, provenance analysis, rifting

#### Abbreviations:

BSE: backscattered electrons  
EDS: energy dispersive X-ray spectrometry  
GEUS: Geological Survey of Denmark and Greenland  
K-S: Kolmogorov-Smirnov  
LA-ICP-MS: laser ablation inductively coupled plasma mass spectrometry  
MDS: multidimensional scaling  
SE: secondary electrons  
SEM: scanning electron microscopy  
TOC: total organic carbon  
XRD: X-ray diffraction

GEUS Bulletin (eISSN: 2597-2154) is an open access, peer-reviewed journal published by the Geological Survey of Denmark and Greenland (GEUS). This article is distributed under a [CC-BY 4.0](https://creativecommons.org/licenses/by/4.0/) licence, permitting free redistribution, and reproduction for any purpose, even commercial, provided proper citation of the original work. Author(s) retain copyright.

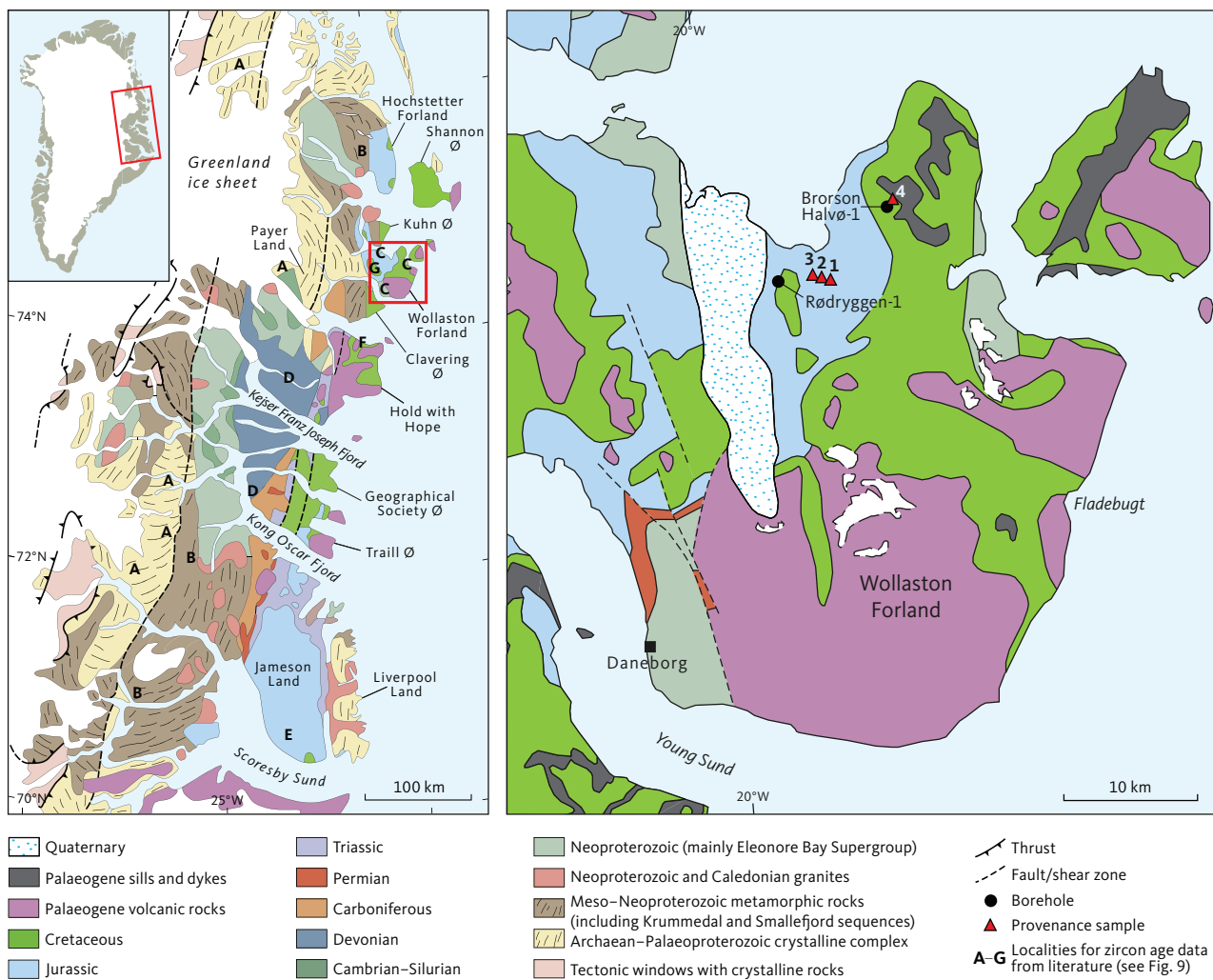
**Edited by:** Jon Ineson & Jørgen Bojesen-Koefoed (GEUS, Denmark)

**Reviewed by:** Chris L. Kirkland (Curtin University, Australia), Kevin Taylor (The University of Manchester, UK)

**Funding:** See page 20

**Competing interests:** See page 20

**Additional files:** See page 20



**Fig. 1** Geological map of North-East Greenland based on Stemmerik *et al.* (1997), Henriksen *et al.* (2008) and Kalsbeek *et al.* (2008a). Detailed map of Wollaston Forland based on the digital Greenland geological map at a scale of 1:500 000 and the printed map series at a scale of 1:100 000. The locations of the Rødryggen-1 and Brorson Halvø-1 boreholes and the samples for zircon U-Pb age dating are shown.

have accumulated in many contemporaneous basins, especially in the northern hemisphere (Langrock *et al.* 2003; Mutterlose *et al.* 2003; Rogov *et al.* 2020), so the findings of this study facilitate the prediction of mudstone composition in such basins.

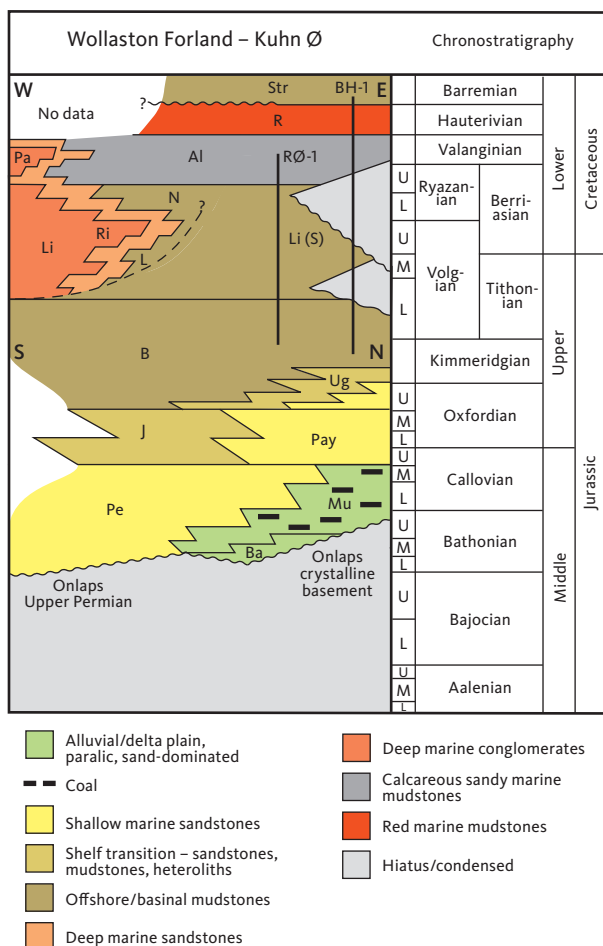
The Rødryggen-1 and Brorson Halvø-1 boreholes were drilled in 2009–2010 to depths of 234.5 and 225.7 m, respectively, covering Kimmeridgian to Barremian sediments (Fig. 2) that represent prolonged mudstone deposition in an evolving half-graben setting. The studied half-graben was bounded by north–south-orientated fault crests delimiting this basin from the rest of the rift system and from the palaeo-coast to the west (Surlyk 1978). Late Jurassic – Early Cretaceous rifting was widespread along the Norwegian–Greenland Seaway, which connected the proto-Arctic to the proto-North Atlantic (e.g. Stoker *et al.* 2017).

We aim to address two main research questions in this study: (1) How do the different phases of half-graben development (i.e. early rift, rift acceleration, rift

climax, waning rift) affect the composition of the deposited sediment in a mudstone-dominated environment? (2) To what extent does the sediment composition differ between the two cores that represent the proximal versus distal parts of the half-graben system?

## 2. Geological setting

The Greenlandic craton consists mainly of crystalline basement, which is exposed at the rim of the Greenland ice sheet and in tectonic windows in the Caledonides (Fig. 1; Henriksen *et al.* 2008; Kalsbeek *et al.* 2008a). The sediment source areas relevant for this study are present within the East Greenland Caledonian fold belt, which originated from the Laurentia–Baltica continental collision that took place in late Cambrian to early Devonian time (McKerrow *et al.* 2000; Smith & Rasmussen 2008). The orogenesis caused westwards thrusting of crystalline complexes of Archaean to Palaeoproterozoic age, metasediments of the Krummedal and Smallefjord sequences of Mesoproterozoic to early Neoproterozoic age, metasediments of the Eleonore



**Fig. 2** Stratigraphic scheme with vertical lines showing the Rødryggen-1 (RØ-1) and Brorson Halvø-1 (BH-1) cored successions. **Al**: Albrechts Bugt Mb. **B**: Bernbjerg Fm. **Ba**: Bastians Dal Fm. **J**: Jakobsstigen Fm. **L**: Laugeites Ravine Mb. **Li**: Lindemans Bugt Formation. **Li (S)**: Lindemans Bugt Fm (Storsletten Mb). **Mu**: Muslingeberg Fm. **N**: Niesen Mb. **Pa**: Palnatokes Bjerg Fm (Young Sund Mb). **Pay**: Payer Dal Fm. **Pe**: Pelion Fm. **R**: Rødryggen Mb. **Ri**: Rigi Mb. **Str**: Stratumbjerg Fm. **Ug**: Ugpik Ravine Mb. Modified from Bojesen-Koefoed *et al.* 2023a, this volume).

Bay Supergroup of Neoproterozoic age and sediments of Neoproterozoic to Silurian age (Kalsbeek *et al.* 2000, 2008b; Watt *et al.* 2000; Thrane 2002; Higgins *et al.* 2004).

Caledonian metamorphism, migmatization and granite intrusion took place in Ordovician to Silurian times, and the crustal thickening resulted in continental sedimentation during the Devonian, followed by post-Caledonian terrestrial and marine sedimentation in the Carboniferous to Palaeogene (Stemmerik *et al.* 1992; Kalsbeek *et al.* 2001; Gilotti *et al.* 2008; Larsen *et al.* 2008). Late Triassic – Middle Jurassic thermal subsidence in the sedimentary basins was followed by Middle Jurassic rifting that was succeeded by transgression in the Late Jurassic and then renewed rifting, which culminated in the latest Jurassic – earliest Cretaceous (Surlyk 2003).

The Wollaston Forland peninsula provides one of the most complete stratigraphic records of the Jurassic and Early Cretaceous in North-East Greenland (Fig. 1). The cored section covers the Kimmeridgian to lower Barremian interval,

which is divided into four formations: (1) the Bernbjerg Formation, (2) the Lindemans Bugt Formation (Storsletten Member), (3) the Palnatokes Bjerg Formation (Albrechts Bugt and Rødryggen Members) and (4) the Stratumbjerg Formation (Fig. 2). The Bernbjerg Formation spans the late Oxfordian to the early Volgian and forms an up to 500–600 m thick black mudstone – shale succession that accumulated in a tectonically-affected shelf setting (e.g. Surlyk *et al.* 2021). Rifting intensified during the Volgian, fragmenting the basin into a series of narrow, 10–30 km wide, westward tilted, fjord-like half-grabens. Major conglomeratic submarine fan-delta systems (Lindemans Bugt Formation, Rigi Member) developed in the most proximal fault block reaching a maximum thickness of 2 km (Surlyk 1978; Henstra *et al.* 2016). The coeval palaeoenvironmental development in more distal fault blocks has remained poorly understood due to lack of outcrops but is well-recorded in the studied cores. The new data indicate deep basinal sedimentation (distal part of Lindemans Bugt Formation) and detachment of the Permpas–Hühnerbjerg Blocks (in which the studied boreholes are located) from the coastal deltaic systems (Hovikoski *et al.* 2023a (this volume), b).

The rift climax lasted until the Valanginian and was followed by waning rift activity and transgression in the western part of the study area (Surlyk 1978, 1984, 1990, 2003). An up to 600 m thick succession of gravity-flow deposits with conglomerates and sandstones (Palnatokes Bjerg Formation, Young Sund Member) accumulated in the proximal fault block, whereas fossiliferous mudstones (Albrechts Bugt and Rødryggen Members) were deposited in basinal areas and on submarine block crests (Surlyk 1978, 1984, 2003; Surlyk & Korstgård 2013; Hovikoski *et al.* 2018). The Rødryggen-1 and Brorson Halvø-1 cores penetrate both mudstone members. New biostratigraphic data (Nøhr-Hansen *et al.* 2020; Alsen *et al.* 2023, this volume) suggest a Valanginian to Hauterivian age for these deposits. Towards the east, fault activity continued until the Barremian and led to the deposition of the coarse-grained Falskebugt Member (Piasecki *et al.* 2020). During the late Hauterivian, deposits of the Palnatokes Bjerg Formation were drowned and succeeded by sub-storm wave-base bioturbated mudstones of the Stratumbjerg Formation (Bjerager *et al.* 2020). A several metres thick upper Hauterivian to lower Barremian interval of the lowermost Stratumbjerg Formation is recorded at the top of the Brorson Halvø-1 core (Alsen *et al.* 2023, this volume) and younger parts of the formation of Barremian to Albian age are present in outcrops near the drill site (Piasecki *et al.* 2020).

### 3. Methodology

#### 3.1 Petrography

The petrographic and mineralogical characteristics of cemented and laminated mudstones in the

Rødryggen-1 and Brorson Halvø-1 cores were studied by transmitted and reflected light microscopy as well as by scanning electron microscopy (SEM). Samples of fracture fillings and sandy intervals were also examined. Polished thin sections were prepared from selected intervals in the cores representing diagenetic features characteristic of the different types of lithologies. The thin sections were impregnated with blue epoxy to ease identification of open pore space. Half of each thin section was etched and stained with sodium cobaltinitrite to facilitate K-feldspar identification. The SEM analyses were performed at the Geological Survey of Denmark and Greenland (GEUS) using a Philips XL40 SEM equipped with a ThermoNoran Energy Dispersive X-ray spectrometry (EDS) detector that was used to analyse the chemistry. Selected samples were studied with a backscattered electron (BSE) detector on carbon-coated thin sections and with a secondary electron (SE) detector on gold-coated rock chips. The mineralogy of each type of lithology present in the Rødryggen-1 and Brorson Halvø-1 cores was analysed by X-ray diffraction (XRD) at the University of Copenhagen, Denmark, and GEUS. The edge of the core was removed to avoid contamination. The bulk mineralogy was measured on a Bruker Advance D8 diffractometer with a Lynx-Eye detector using samples crushed to <math><63\ \mu\text{m}</math> applying the Bragg–Brentano method. Semi-quantification of the bulk mineralogy was obtained by the Rietveld method (Rietveld 1969; McCusker *et al.* 1999). The clay fraction analysis was carried out on a Philips 1050 goniometer with fixed divergence, anti-scatter slits and Co-K $\alpha$  radiation (pulse high selection and Fe-filter). Chemical pre-treatment with NaOCl at pH 9.0 was used to remove organic matter. The samples were dispersed ultrasonically in distilled water to acquire the clay fraction (<math><2\ \mu\text{m}</math>). The >math>>30\ \mu\text{m}</math> fraction was removed by density separation and the intermediate fraction by centrifugation in a centrifugal particle size analyser (Slater & Cohen 1962). The suspensions were flocculated in 1 M NaCl, and excess salt was removed by centrifugation and washing with water and ethanol. Three orientated specimens were made for each sample by the pipette method, comprising Mg-saturated air-dry, Mg-saturated with glycerol, and K-saturated air-dry heated at 300°C for 1 h. An X-ray diffractogram was produced for each of the saturated specimens on which the discrete minerals were identified from peak positions (Hillier 2000) and semi-quantified by application of correction factors.

### 3.2 Zircon U-Pb geochronology

The Rødryggen-1 and Brorson Halvø-1 cores did not contain sufficiently coarse material to apply detrital

zircon U-Pb age dating methods. Instead, outcrop samples collected from three locations east of the Rødryggen-1 drill site and a location situated north-east of the Brorson Halvø-1 drill site were used for the provenance analysis (Fig. 1). The samples collected near the Rødryggen-1 drill site consist of silty sandstone to sandy siltstone belonging to the Bernbjerg Formation, corresponding to the lower part of the cored succession. The sandstone sampled near the Brorson Halvø-1 drill site belongs to the Albian part of the Stratumbjerg Formation, so it is younger than the part of the formation encountered in the Brorson Halvø-1 core. The detrital zircon U-Pb age analyses were performed by laser ablation inductively coupled plasma mass spectrometry (LA-ICP-MS) at GEUS. Samples were crushed and sieved to retrieve the grain-size fraction <math><500\ \mu\text{m}</math>. A water-shaking Wilfley table was used to obtain heavy mineral concentrates. Zircon grains were hand-picked in a random way to ensure that a range of grain sizes, shapes and colours were included. The polished epoxy mount with the zircon grains was cleaned in an ultrasonic bath with propanol and loaded into the sample cell of the laser ablation system for radiometric age dating. The data were acquired with a single spot analysis on individual zircon grains. A beam diameter of 30  $\mu\text{m}$  and a crater depth of *c.* 15–20  $\mu\text{m}$  were used. The amount of ablated material was *c.* 200–300 ng for the ablation time of 30 sec. The ablated material was analysed on an Element2 (Thermo Finnigan) single-collector, double focusing, magnetic sector-field, inductively coupled plasma mass spectrometer with a fast-field regulator for increased scanning speed. The total acquisition time was 60 sec for each analysis, of which the first 30 sec were used to measure the gas blank. The instrument was tuned to give large, stable signals for the  $^{206}\text{Pb}$  and  $^{238}\text{U}$  peaks, low background count rates (typically around 150 counts per second for  $^{207}\text{Pb}$ ) and low oxide production rates ( $^{238}\text{U}^{16}\text{O}/^{238}\text{U}$  generally below 2.5%).  $^{202}\text{Hg}$ ,  $^{204}(\text{Pb}+\text{Hg})$ ,  $^{206}\text{Pb}$ ,  $^{207}\text{Pb}$ ,  $^{208}\text{Pb}$ ,  $^{232}\text{Th}$  and  $^{238}\text{U}$  intensities were determined through peak jumping using electrostatic scanning in low resolution mode and with the magnet resting at  $^{202}\text{Hg}$ . Mass  $^{202}\text{Hg}$  was measured to monitor the  $^{204}\text{Hg}$  interference on  $^{204}\text{Pb}$  where the  $^{202}\text{Hg}/^{204}\text{Hg} \equiv 4.36$ , which can be used to correct significant common Pb contributions using the model Pb composition of Stacey & Kramers (1975).

Standard-sample bracketing using the GJ-1 zircon (Jackson *et al.* 2004) was used to correct the elemental fractionation induced by the laser ablation and the instrumental mass bias on measured isotopic ratios. Long-term external reproducibility was monitored by repeated analyses of the Plešovice zircon standard (Sláma *et al.* 2008). The reported ages are based on

$^{207}\text{Pb}/^{206}\text{Pb}$  derived ages for the >0.8 Ga (billion years) analyses and  $^{206}\text{Pb}/^{238}\text{U}$  ages for the <0.8 Ga analyses, since the latter is more precise for the younger age range, and a natural gap between age populations exists. The propagation of the analytical errors follows the principles of Sambridge & Lambert (1997). Age measurements were discarded if they lacked a stable  $^{207}\text{Pb}/^{206}\text{Pb}$  plateau or for U/Pb or Pb/Pb error >10%. A correction for common Pb was applied on a small fraction ( $\leq 7\%$ ) of the concordant analyses from each sample. The data are plotted using kernel density estimation (Vermeesch 2012) employing analyses with <10% discordance. The analytical data are reported in Supplementary File S1.

## 4. Results

### 4.1 Lithology

The studied succession was deposited during a protracted rifting episode that is differentiated into four discrete rift phases: (1) early rifting during the Kimmeridgian part of the Bernbjerg Formation, (2) rift acceleration during the Volgian part of the Bernbjerg Formation, (3) rift climax during deposition of the Lindemans Bugt Formation and (4) waning rifting during deposition of the Palnatokes Bjerg Formation (Figs 3 and 4; Surlyk 1978, 2003). These major rift phases resulted in significant shifts in depositional conditions that are reflected in the lithological characteristics observed in the different stratigraphic units in the Rødryggen-1 and Brorson Halvø-1 cores.

In the cored sections, the Bernbjerg Formation comprises dark grey mudstones with interlaminated coarse siltstones to very fine sandstones in some intervals (Fig. 5A). The Lindemans Bugt Formation consists of dark grey clayey mudstones (Fig. 5C) with a larger content of fossils and pyrite than in the Bernbjerg Formation. The Albrechts Bugt Member of the Palnatokes Bjerg Formation comprises light grey mudstones (Fig. 5D) that differ from the Lindemans Bugt Formation in being more calcareous, sandy and bioturbated. The Rødryggen Member of the Palnatokes Bjerg Formation consists of red hematitic mudstones with intercalated sandy mudstones (Fig. 5E). The Stratumbjerg Formation contains bioturbated grey mudstones (Fig. 5F). The sedimentological characteristics are described in more detail by Hovikoski *et al.* (2023a, this volume).

Carbonate-cemented intervals occur in all the stratigraphic units and are characterised by lower gamma-ray values (Figs 3, 4) and lighter colours (Fig. 5B). The lighter colours are also evident in the microscopic appearance of the cemented mudstones due to the lower clay mineral content as compared to the uncemented mudstones (Figs 6A, 6B). Pyrite is evident in many core intervals as well as various macrofossils, deformation structures, faults and fractures (Figs 3 and 4).

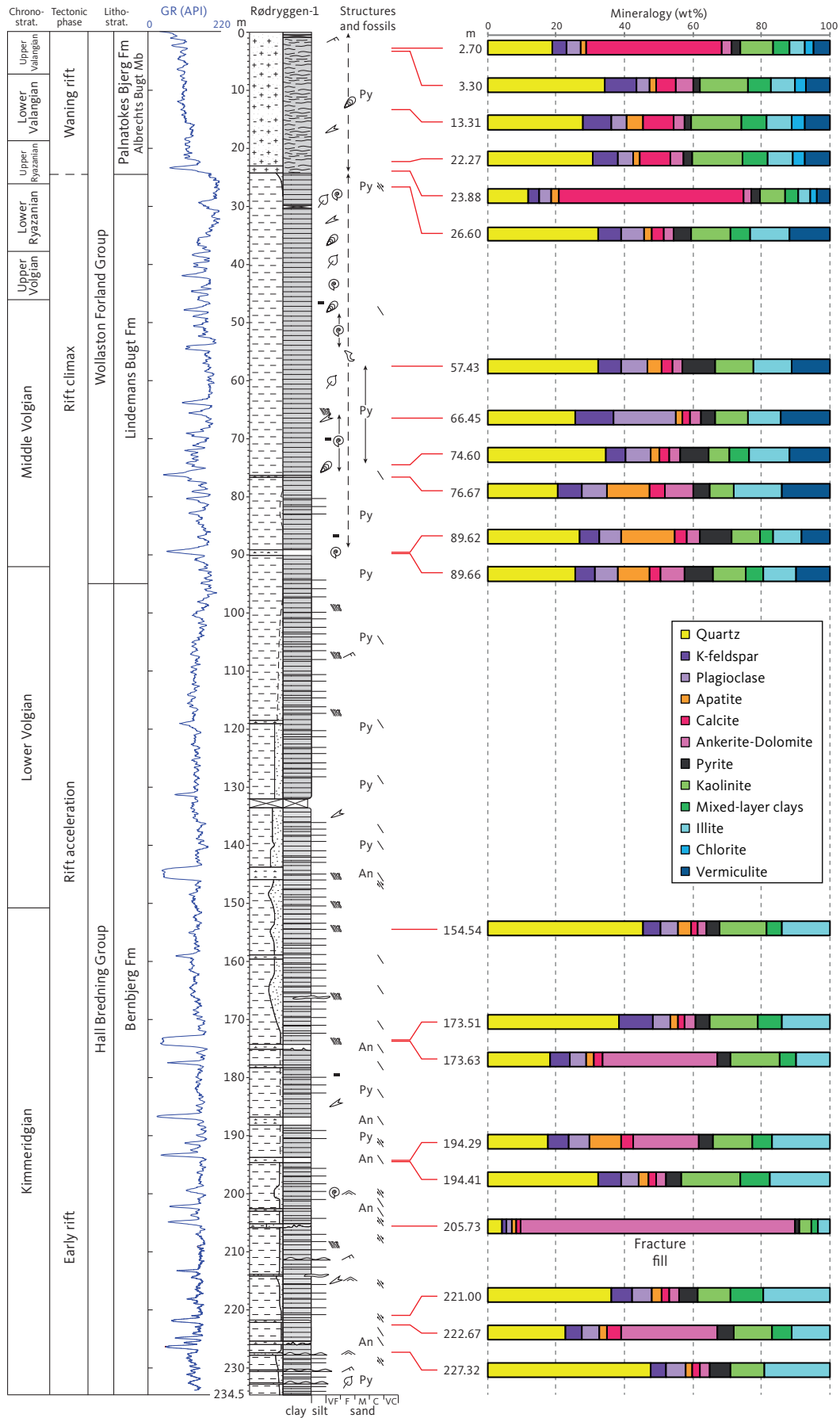
### 4.2 Detrital components

The mineralogy of the Rødryggen-1 and Brorson Halvø-1 cores based on XRD analyses is presented in Figs 3 and 4 for the 27 analysed mudstones and two samples of cemented fractures. Quartz is the most abundant mineral amounting to 12–48 wt% with an average of 29 wt%, which is present as silt- and sand-sized grains in the mudstones (Fig. 6C). K-feldspar and plagioclase/albite occurs in amounts of up to 11 and 18 wt%, respectively, and each of them are present as 6 wt% on average. Petrographic analysis of the K-feldspar grains reveals that they are generally well-preserved, whereas the plagioclase and albite grains are often partially dissolved (Fig. 6D). Apatite is found as detrital clasts (Fig. 6E) in amounts of 4 wt% on average with the highest contents up to 16 wt% occurring in a condensed interval in the lower part of Lindemans Bugt Formation in the Rødryggen-1 core.

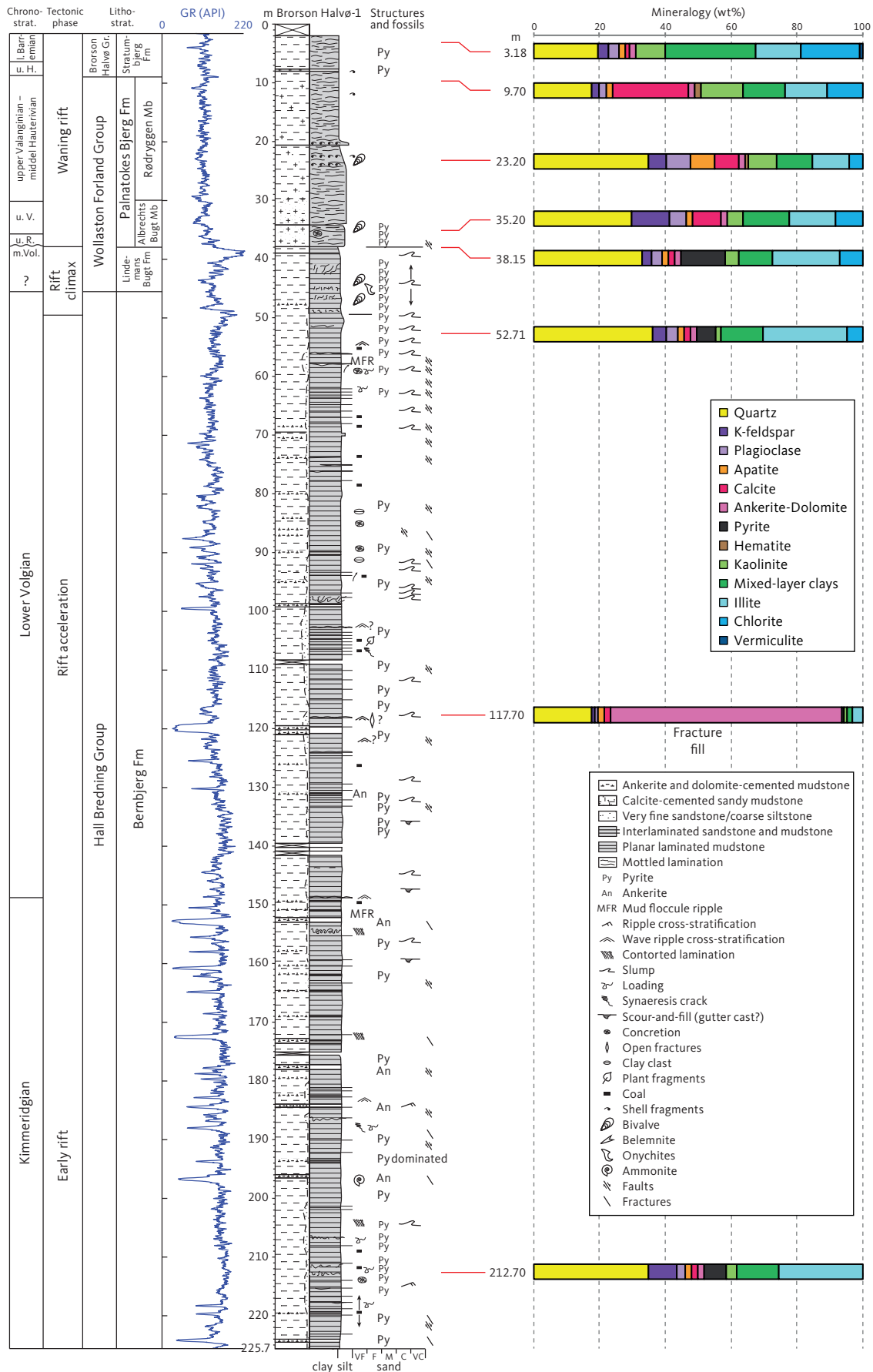
Calcite is present as detrital clasts, including bioclasts in the Palnatokes Bjerg Formation, in both the Albrechts Bugt and Rødryggen Members. The Bernbjerg and Lindemans Bugt Formations are rich in organic matter including some coal fragments. Detrital heavy minerals are found in accessory amounts and comprise primarily ilmenite, leucoxene, rutile, magnetite, zircon and garnet in the form of almandine. Muscovite could not be differentiated from illite by XRD but was observed in thin section. The mica minerals primarily consist of muscovite with subordinate biotite. The micas are generally aligned parallel to the lamination and are often cleaved into thin sheets and bend around less ductile grains (Fig. 6C).

Most of the clay minerals are detrital as testified by the absence of growth structures and by their tangential orientation around the other detrital minerals (Fig. 6F). Kaolinite is present in the matrix of all the mudstones and occurs in higher amounts in the Rødryggen-1 core than in the Brorson Halvø-1 core (Figs 3, 4). Kaolinite is found in amounts up to 17 wt% with an average of 10 wt%. Mixed-layer illite-smectite is found in amounts of 7 wt% on average with the highest contents occurring in the Brorson Halvø-1 core and especially in the sample from the Stratumbjerg Formation where it constitutes 28 wt%. Illite occurs with an average of 13 wt% and is more abundant overall in the Brorson Halvø-1 core than in the Rødryggen-1 core. The smallest illite contents within each well occur in the Palnatokes Bjerg Formation and the highest contents of up to 25 wt% are present in the Bernbjerg Formation. Some of the illite is authigenic as evident by its morphology, but the proportion of detrital to authigenic illite cannot be quantified.

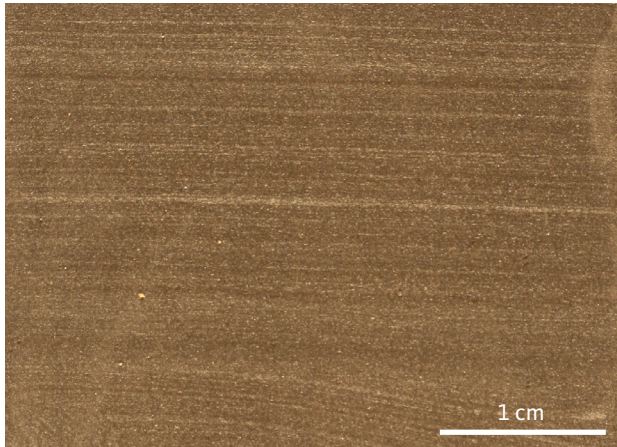
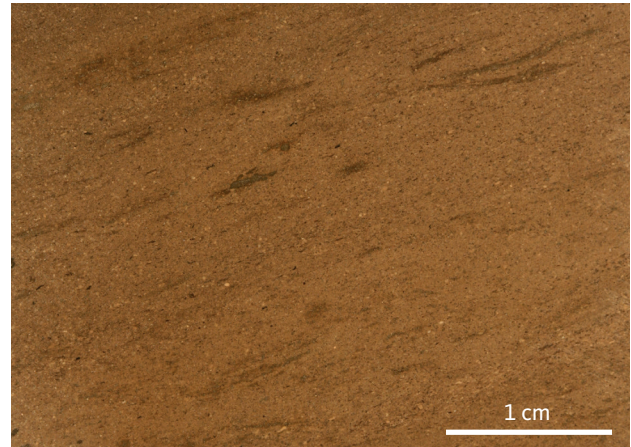
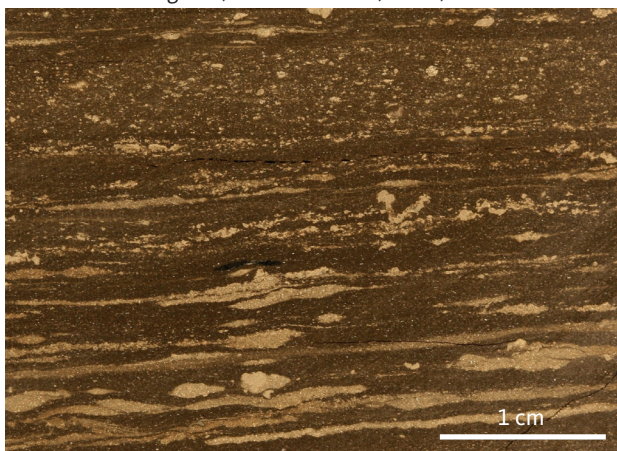
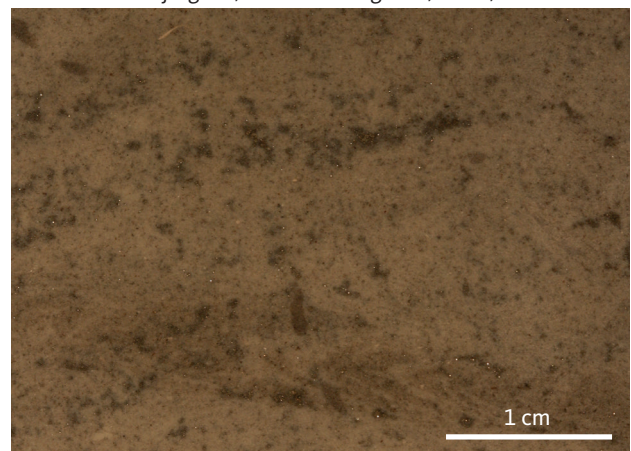
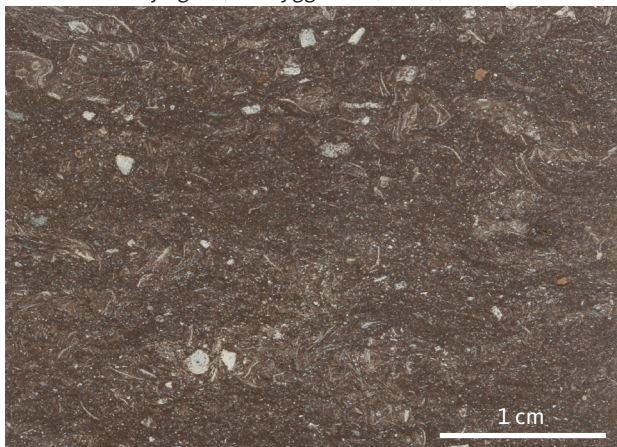
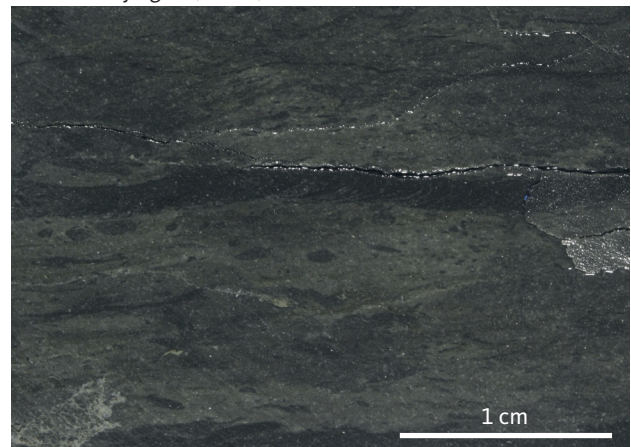
Chlorite is found in all samples from the Brorson Halvø-1 core (Fig. 6F), except the two deepest samples from the Bernbjerg Formation, and its content increases



**Fig. 3** Mineralogy from XRD of the Rødryggen-1 core plotted with the sedimentological log. Chronostratigraphy from Alsen *et al.* (2023, this volume). See Fig. 4 for legend. **Chronostrat.:** chronostratigraphy. **Lithostrat.:** lithostratigraphy. **GR:** gamma ray. **API:** American Petroleum Units.



**Fig. 4** Mineralogy from XRD of the Bronson Halvø-1 core shown alongside the sedimentological log. Chronostratigraphy from Alsen *et al.* (2023, this volume). **Chronostrat.:** chronostratigraphy. **Lithostrat.:** lithostratigraphy. **GR:** gamma ray. **API:** American Petroleum Units.

**A** Bernbjerg Fm, RØ-1, ~166 m**B** Lindemans Bugt Fm, Storsletten Mb, RØ-1, ~76.6 m**C** Lindemans Bugt Fm, Storsletten Mb, RØ-1, ~64 m**D** Palnatokes Bjerg Fm, Albrechts Bugt Mb, RØ-1, ~2.7 m**E** Palnatokes Bjerg Fm, Rødryggen Mb, BH-1, ~20 m**F** Stratumbjerg Fm, BH-1, ~2 m

**Fig. 5** Core photos of the mudstone texture of cemented versus uncemented mudstones. **BH-1:** Brorson Halvø-1 core. **RØ-1:** Rødryggen-1 core. **A:** Laminated sandy mudstone. **B:** Cemented mudstone. **C:** Laminated pyritic mudstone. **D:** Bioturbated mudstone. **E:** Bioclastic hematitic cemented mudstone. **F:** Bioturbated mudstone.

upwards with the highest amount of 18 wt% occurring in the Stratumbjerg Formation (Figs 3, 4). In the Rødryggen-1 core, chlorite is only present in the Palnatokes Bjerg Formation where it occurs in amounts of 2–4 wt%. Vermiculite is not present in the mudstones from the Brorson Halvø-1 core except for a small content (1 wt%) in the Stratumbjerg Formation. In the Rødryggen-1 core,

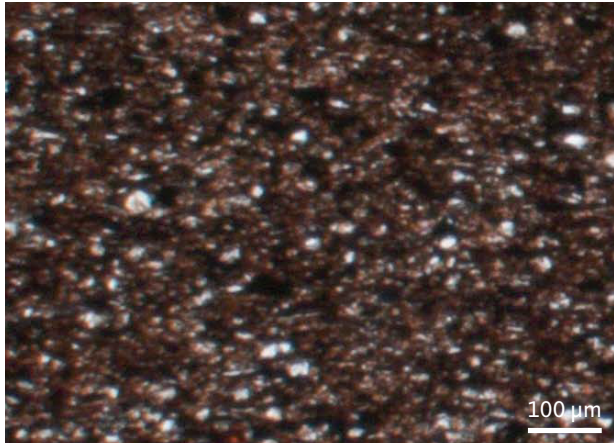
vermiculite is present in all samples from the Lindemans Bugt and Palnatokes Bjerg Formations in contents of 4–14 wt%, whereas it is absent in the Bernbjerg Formation.

#### 4.3 Authigenic minerals

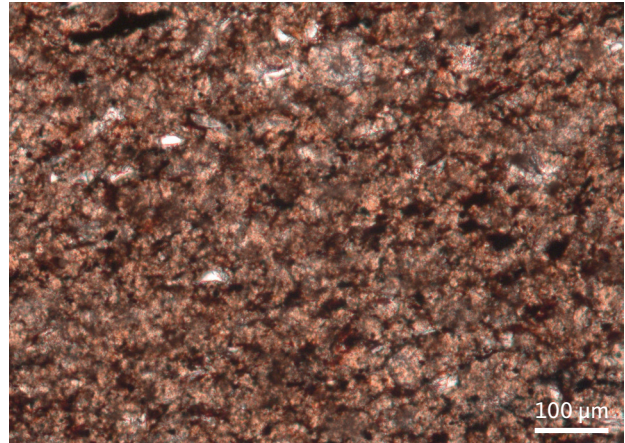
Pyrite is on average 5 wt% and it was the first mineral that precipitated in the sediments. Pyrite is present



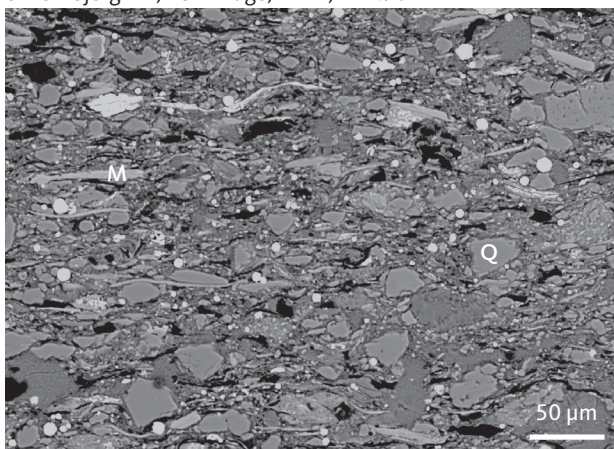
**A** Bernbjerg Fm, TL image, RØ-1, 201.81 m



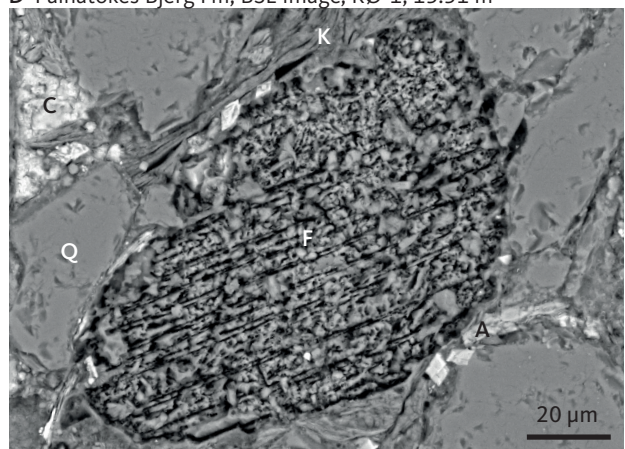
**B** Bernbjerg Fm, TL image, RØ-1, 187.50 m



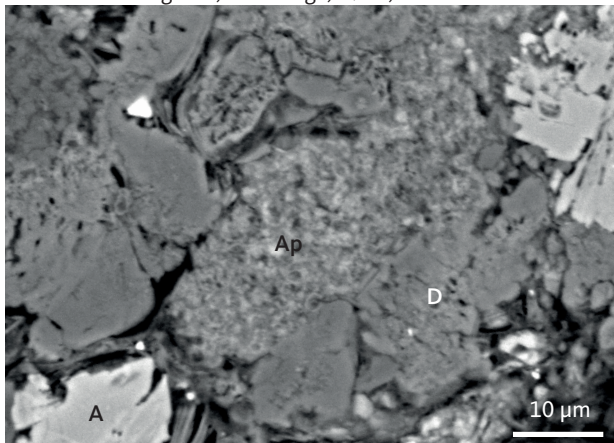
**C** Bernbjerg Fm, BSE image, BH-1, 212.70 m



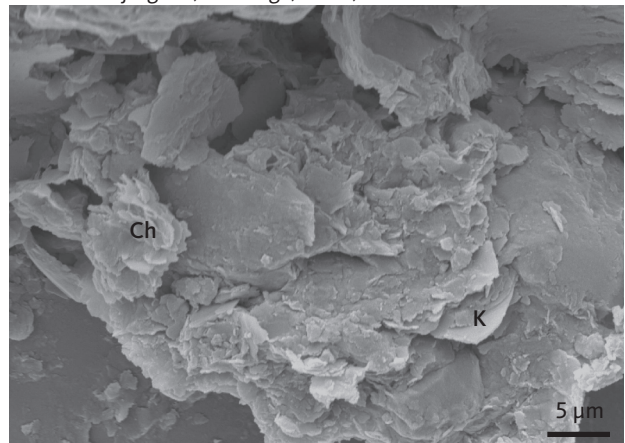
**D** Palnatokes Bjerg Fm, BSE image, RØ-1, 13.31 m



**E** Lindemans Bugt Fm, BSE image, RØ-1, 89.96 m



**F** Stratumbjerg Fm, SE image, BH-1, 3.18 m



BH-1: Brorson Halvø-1 core  
 RØ-1: Rødryggen-1 core  
 TL: transmitted light

CN: crossed nicols  
 BSE: backscattered electron  
 SE: secondary electron

A: ankerite  
 Ap: apatite  
 B: barite

C: calcite  
 Ch: chlorite  
 D: dolomite  
 F: feldspar  
 K: kaolinite  
 M: mica  
 ML: mixed-layer clay  
 O: opal  
 Om: organic matter  
 Pe: pyrite euhedra  
 Pf: pyrite framboid  
 Q: quartz

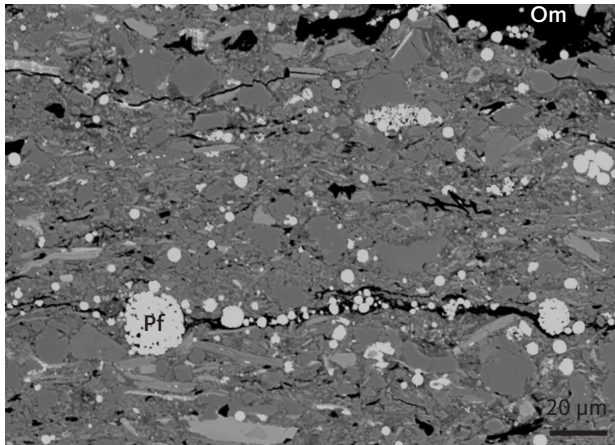
**Fig. 6** Texture and detrital phases. **A:** Typical mudstone texture. **B:** Cemented mudstone texture. **C:** Quartz occurs as silt- and sand-sized grains in the mudstones. **D:** Partially dissolved albite grain. **E:** Apatite occurs as detrital clasts. **F:** Most clay minerals are detrital such as chlorite.

in all formations except some parts of the Stratumbjerg and Palnatokes Bjerg Formations in the Brorson Halvø-1 core (Figs 3, 4). It is often found in association with organic matter (Fig. 7A). The highest amounts (4–14 wt%) are found in the Lindemans Bugt Formation where the pyrite framboids are often overgrown by

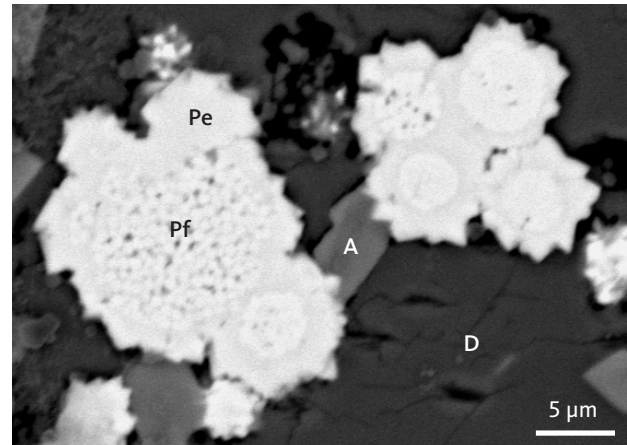
euhedral pyrite (Fig. 7B). Only framboidal pyrite is present in the remaining formations where it constitutes 4–7 wt% in the Bernbjerg Formation and 0–3 wt% in the Palnatokes Bjerg Formation.

Although the kaolinite crystals have euhedral shapes, they are likely to have been transported before

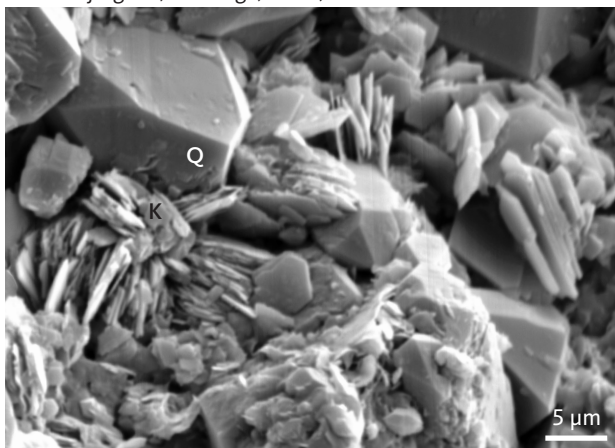
A Bernbjerg Fm, BSE image, BH-1, 52.71 m



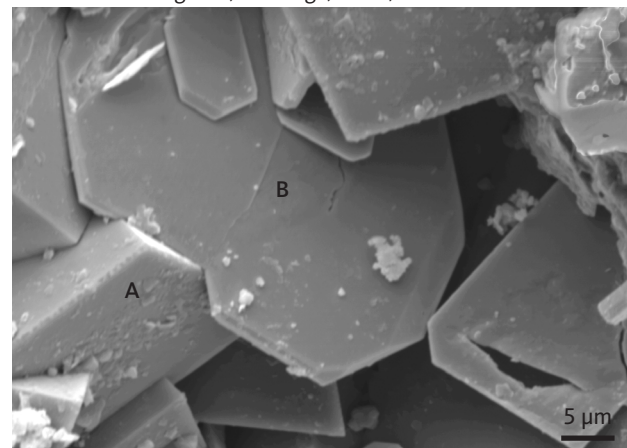
B Lindemans Bugt Fm, BSE image, RØ-1, 76.47 m



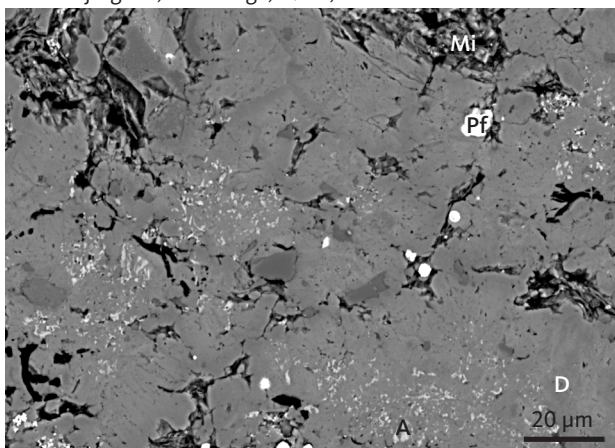
C Bernbjerg Fm, SE image, RØ-1, 227.32 m



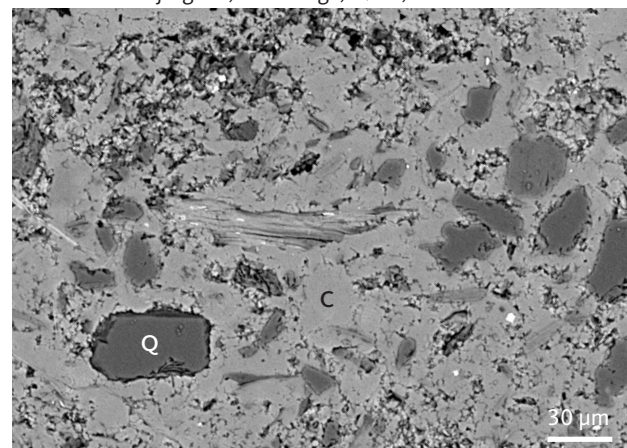
D Lindemans Bugt Fm, SE image, RØ-1, 90.01 m



E Bernbjerg Fm, BSE image, RØ-1, 187.50 m



F Palnatokes Bjerg Fm, BSE image, RØ-1, 23.88 m



**Fig. 7** Authigenic minerals. **A:** Framboidal pyrite has often formed in connection with organic matter. **B:** Euhedral pyrite has only formed in Lindemans Bugt Formation where it has overgrown pyrite framboids. **C:** Quartz has overgrown detrital kaolinite. **D:** Barite has overgrown ankerite rhombs. **E:** Dolomite is the dominant carbonate cement in Bernbjerg and Lindemans Bugt Formations. **F:** Calcite is the dominant carbonate cement in Palnatokes Bjerg Formation. See Fig. 6 for abbreviations.

deposition since they do not occur in well-defined booklets (Fig. 7C). However, some detrital grains have been kaolinised, including some of the muscovite and feldspar grains, which must have happened within the sediment since they would have disintegrated during transport. It is often difficult to distinguish unambiguously between the detrital and authigenic clay minerals,

but the morphology of the mixed-layer illite-smectite and illite indicate that part of it is authigenic. Fibrous and hairy illite was observed using SEM. Thin quartz overgrowths have mainly precipitated in the coarser-grained intervals (Fig. 7C) and overgrow pyrite and kaolinite. Barite has precipitated in some of the mudstones where it formed as the last authigenic phase.

It occurs as string-like precipitations and as euhedral crystals overgrowing ankerite (Fig. 7D). Barite was identified by EDS but has formed in such small amounts that it could not be estimated by XRD analysis.

Pervasive carbonate cementation of the mudstones is found in some intervals of all the studied formations, and these intervals are characterised by low gamma-ray values in the natural gamma log (Figs 3, 4). High concentrations of bioclasts or micrite are present in the carbonate-cemented intervals, except for those with siderite. Dolomite is the dominant carbonate mineral in the Bernbjerg and Lindemans Bugt Formations, whereas calcite is dominant in the Palnatokes Bjerg Formation and siderite is dominant in the Stratumbjerg Formation.

Dolomite and ankerite could not be clearly discriminated by XRD so they have been grouped as ankerite-dolomite in the XRD results (Figs 3, 4). However, both minerals are present since they were identified by EDS. They are found in all formations with the highest abundance in the Bernbjerg Formation (maximum 34 wt%) followed by Lindemans Bugt Formation (maximum 8 wt%). Poikilotopic dolomite occurs in highest abundance, whereas ankerite occurs mostly as smaller rhombs (Fig. 7E). Ankerite is often precipitated between exfoliated mica flakes. An outwards increase in Fe content is observed in both the dolomite and ankerite crystals.

Calcite occurs in amounts of 2–4 wt% in the samples from the Bernbjerg and Lindemans Bugt Formations, reaching 6–54 wt% in the Palnatokes Bjerg Formation comprising both detrital and authigenic calcite that is poikilotopic and micritic (Fig. 7F). A calcite content of 1 wt% is found in the sample from the Stratumbjerg Formation. This sample does not contain siderite, but it is present in other samples from this stratigraphic unit where it has precipitated as an early phase.

#### 4.4 Bioclasts

The Bernbjerg and Lindemans Bugt Formations contain numerous calpionellids that are most abundant in the cemented mudstones. The calpionellids and other shell material in the Bernbjerg and Lindemans Bugt Formations are recrystallised, but moulds of molluscs and ammonites have been found (Alsen *et al.* 2023). Calpionellids are calcareous microfossils of uncertain affinity. They have oblong shells which have been filled with either dolomite or micritic calcite and often also ankerite and pyrite (Fig. 8A). Pyrite precipitated mostly along shell rims though sometimes filling most of the internal cavity. Ankerite formed small euhedral crystals, most of which precipitated on the exterior of the bioclasts. Poikilotopic dolomite crystals precipitated in most of the remaining cavity, but some porosity is often preserved (Fig. 8B).

Fossils in the Palnatokes Bjerg Formation include ostracods, brachiopods, foraminifera and inoceramid bivalves (Alsen *et al.* 2023). The formation contains abundant calcispheres, especially in the cemented intervals. They have not been recrystallised as seen by the characteristic test (Fig. 8C) and by the extinction pattern following the growth structure in other fossils. These calcispheres are probably calcareous dinoflagellate cysts and have a spherical test. Calcite has precipitated in the interior, and small ankerite crystals have sometimes formed within the calcite (Fig. 8D).

#### 4.5 Fractures

Small fractures are present in most of the core and are most evident in the cemented intervals where they cut through the carbonate-cemented fabrics. Opal has often formed along the rims of the fractures where it radiates in multiple layers and forming spherical layers around a protruding matrix (Fig. 8E). The remaining parts of the fractures are filled with dolomite in which the Fe content decreases towards the middle of the fractures (Fig. 8F). The dolomite has occasionally replaced some of the opal along its outer rim (Fig. 8E).

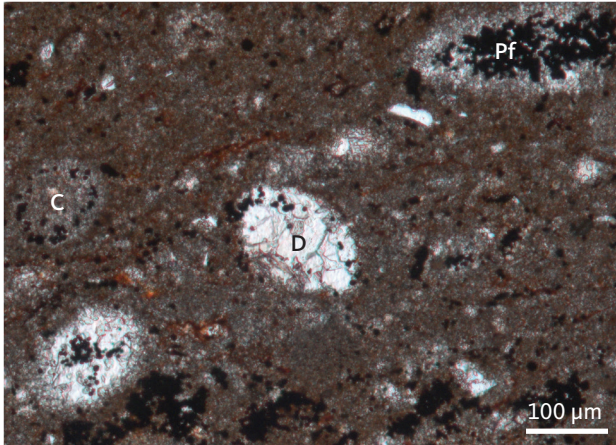
XRD analyses have been made of fracture fills comprising one sample selected from each well in the Bernbjerg Formation where fractures are most abundant, and show that dolomite is the dominant fracture-filling cement (Figs 3, 4). Fracturing has happened several times as seen by the cross-cutting relationships of the fracture generations, where each of them became cemented prior to the next generation of successively wider fractures. The largest encountered fractures are up to a few centimetres wide. The last generation of fractures were not filled by any minerals and thus increased the porosity and permeability.

#### 4.6 Zircon U-Pb ages

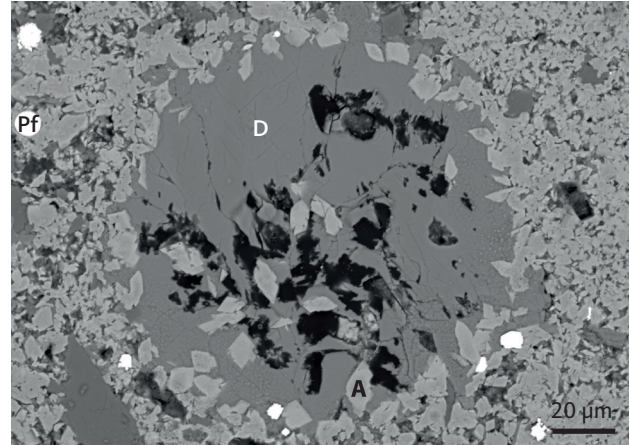
The detrital zircon U-Pb ages of the four outcrop samples from Wollaston Forland (Fig. 1) cover a broad Mesoproterozoic to Palaeozoic age span (Fig. 9). The discordant ages (comprising 21–28%) are not plotted but included in Supplementary File S1. The three samples from the Bernbjerg Formation (samples 1–3, Fig. 9) all contain a pronounced Archaean zircon age population with peak ages at 2.75–2.65 Ga (comprising 7–10% in each sample), whereas only a single Archaean zircon grain was found in the sample from the Stratumbjerg Formation (sample 4, Fig. 9).

The dominant age populations of the samples are present within the 2.0–1.6 Ga interval (comprising 42–75% in each sample), although the relative proportions between the age populations vary. In the

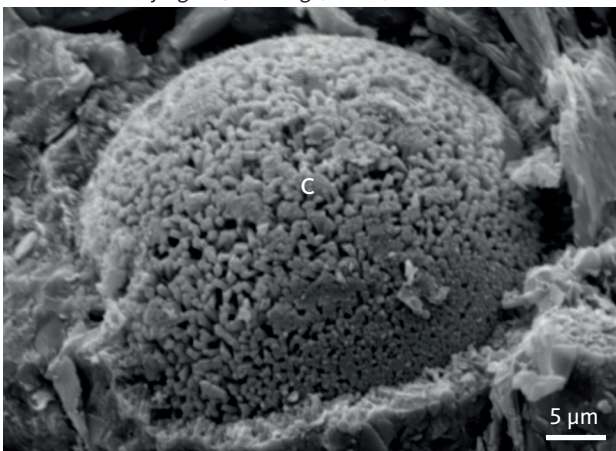
A Lindemans Bugt Fm, TL image, RØ-1, 76.47 m



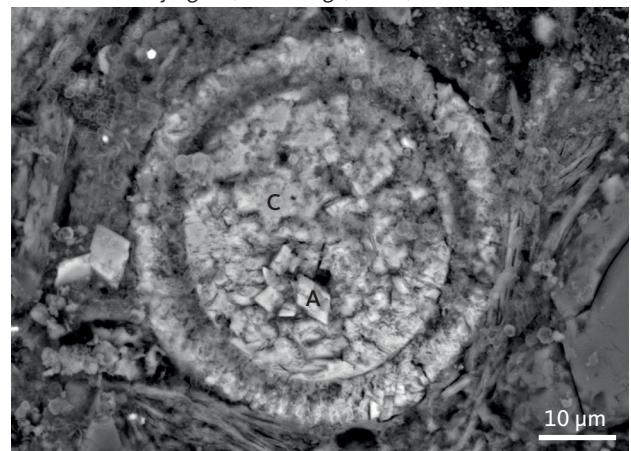
B Lindemans Bugt Fm, BSE image, RØ-1, 76.47 m



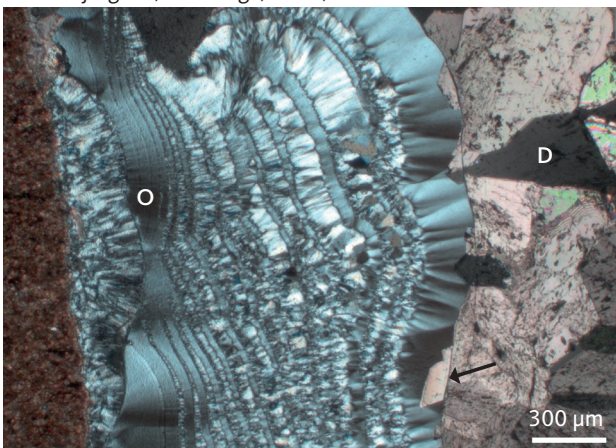
C Palnatokes Bjerg Fm, SE image, RØ-1, 13.31 m



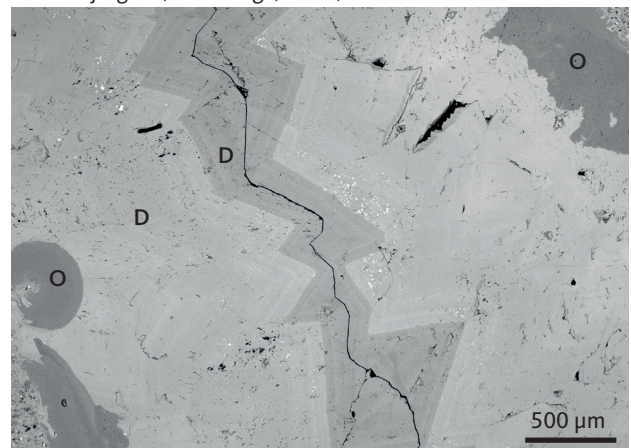
D Palnatokes Bjerg Fm, BSE image, RØ-1, 13.31 m



E Bernbjerg Fm, CN image, RØ-1, 187.50 m



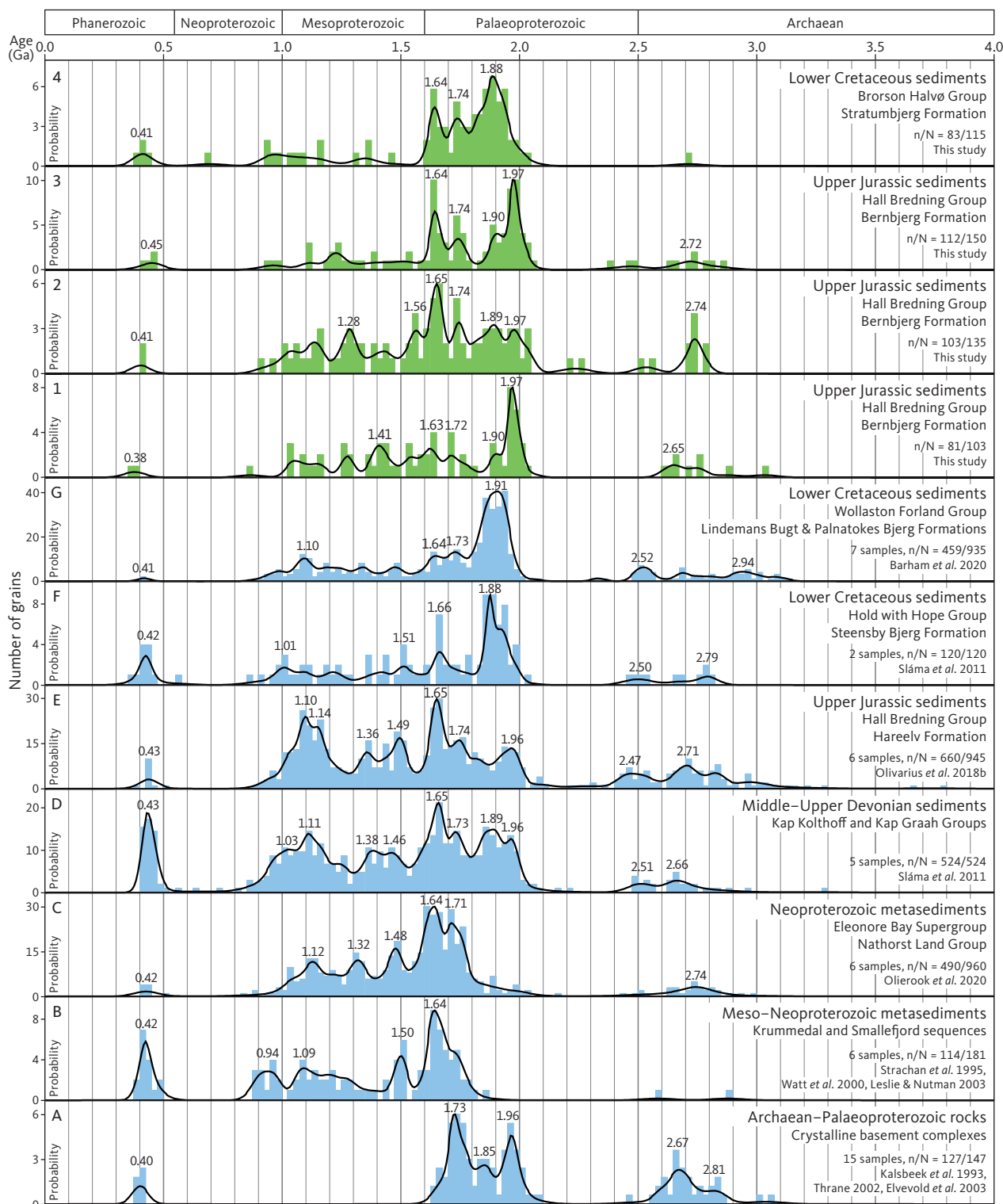
F Bernbjerg Fm, BSE image, RØ-1, 187.50 m



**Fig. 8** Bioclasts and fracture fillings. **A–B:** Recrystallised calpionellids filled with combinations of calcite, dolomite, ankerite and pyrite, and occasionally with internal porosity. Calpionellids are present in Bernbjerg and Lindemans Bugt Formations. **C–D:** Well-preserved calcispheres filled with calcite and small ankerite rhombs. Calcispheres are present in Palnatokes Bjerg Formation. **E:** Opal precipitated in several zones in a fracture and succeeded by dolomite, which has replaced some opal along the contact (**arrow**). **F:** Opal along fracture rims and succeeded by dolomite with lower Fe content in the middle. Fractures are most abundant in Bernbjerg Formation. See Fig. 6 for abbreviations.

Bernbjerg Formation, an age population with peak age at 1.97 Ga is dominant in two of the samples (samples 1 and 3, comprising 23–24%) and evident in the third (sample 2, comprising 10%), but not in the sample from the Stratumbjerg Formation. The dominant age population in the Stratumbjerg Formation sample has peak

age at 1.88 Ga (sample 4, comprising 39%), and this population is less pronounced and slightly older in the Bernbjerg Formation samples. An age population with peak ages at 1.65–1.63 Ga is pronounced in the sample from Stratumbjerg Formation (sample 4, comprising 17%) and in two of the samples from the Bernbjerg



**Fig. 9** Zircon U-Pb age distributions of the Upper Jurassic – Lower Cretaceous sediments (**1–4**) compared to selected zircon ages from the region (**A–G**: Strachan *et al.* 1995; Watt *et al.* 2000; Thrane 2002; Elvevold *et al.* 2003; Kalsbeek *et al.* 1993; Leslie & Nutman 2003; Sláma *et al.* 2011; Olivarius *et al.* 2018b; Barham *et al.* 2020; Olierook *et al.* 2020). The Phanerozoic zircon ages in A–C are from the intruded Caledonian granites. The sampling locations are shown in Fig. 1. The ages are plotted using kernel density estimation (Vermeesch 2012) and histograms with a bin interval of 25 million years. Zircon ages with <10% discordancy are plotted. “n/N” denotes the number of concordant analyses out of the total number of analyses. See Fig. 1 for locations.

Formation (samples 2 and 3, both comprising 16%). A population with peak age of 1.74 Ga is slightly less prominent in the same three samples (comprising 9–14% in each sample), whereas both age populations

are less prominent in the last sample from the Bernbjerg Formation (sample 1; Fig. 9).

A wide range of Mesoproterozoic zircon ages are found in all four samples (comprising 11–38% in each

sample) with less pronounced age populations as compared to the Palaeoproterozoic populations. Few Neoproterozoic zircons are encountered (comprising 1–6% in each sample), and an age gap occurs at 0.9–0.5 Ga except for a few grains (Fig. 9). Small Palaeozoic age populations of 2–4 grains are found in all samples with peak ages varying between 0.45 and 0.38 Ga (comprising 2–5% in each sample). The oldest and youngest of these Ordovician–Devonian zircons, with ages of  $474 \pm 14$  Ma and  $364 \pm 3$  Ma, respectively, are both from the Bernbjerg Formation.

## 5. Discussion

### 5.1 Provenance analysis

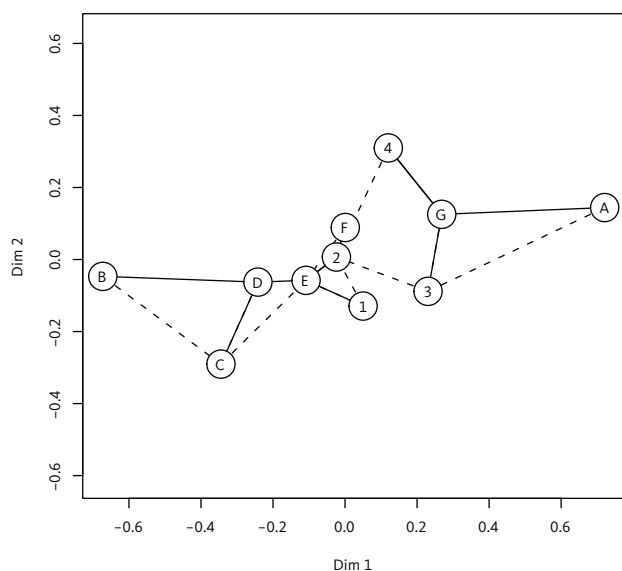
The Mesoarchaeo to Palaeozoic zircon age populations found in the four analysed samples of Upper Jurassic – Lower Cretaceous sediments from Wollaston Forland are comparable (Fig. 9). The age distributions of the studied sediments are all characterised by a dominance of 2.0–1.6 Ga ages and by containing the full range of zircon ages within this time interval, although the relative proportion between the probabilities of the age populations varies. Therefore, the sediments presumably have the same overall provenance in which the proportion between the Palaeoproterozoic zircon ages varies. However, some of the differences in age distributions between the samples may possibly be the result of bias related to mineral separation with handpicking of grains for analysis (e.g. Sláma & Košler 2012; Dröllner *et al.* 2021). Selected zircon age data from the literature are plotted in Fig. 9 to facilitate comparison with possible sediment source rocks.

As in the studied sediments, zircon age populations with a dominance of 2.0–1.6 Ga ages occur in Lower Cretaceous and Lower Triassic sediments from northern Hold with Hope, c. 80 km south-south-west of the study area (Fig. 1; Fonneland *et al.* 2004; Sláma *et al.* 2011). These sediments also contain Archaean, Mesoproterozoic and Palaeozoic age populations with low probabilities, although the Palaeozoic peak age is more pronounced than in the studied sediments (Fig. 9). The age populations of Upper Jurassic sediments from southern Jameson Land c. 450 km south-south-west of the study area are similar overall to the studied sediments, but with significantly larger relative proportions of the Archaean and Mesoproterozoic age populations (Olivarius *et al.* 2018b). Lower Jurassic sediments from southern Jameson Land have a significantly different age distribution; they exhibit a limited number of peak ages reflecting their local provenance from the Liverpool Land High that was elevated at the time (Sláma *et al.* 2011).

The zircon age populations of Carboniferous and Devonian sediments along Kong Oscar Fjord and inner Kejser Franz Joseph Fjord (Moskusokse Fjord) are comparable to those in the studied sediments, except that the Mesoproterozoic and Palaeozoic populations are more prominent in these older sediments; furthermore, Archaean ages are more common in the Carboniferous sediments (Sláma *et al.* 2011). The Neoproterozoic Lyell Land Group and Nathorst Land Group of the Eleonore Bay Supergroup have age distributions that are distinctly different from each other (Watt *et al.* 2000; Dhuime *et al.* 2007; Sláma *et al.* 2011; Olierook *et al.* 2020). Late Mesoproterozoic zircons are dominant in the Lyell Land Group along inner Kong Oscar Fjord (Segelsellskapet Fjord) with subordinate early Mesoproterozoic zircons, so these sediments show poor resemblance to the studied Upper Jurassic – Lower Cretaceous sediments. The Nathorst Land Group is dominated by late Palaeoproterozoic age populations and additionally contains several Mesoproterozoic age populations in addition to a smaller Archaean population; a sample of the intruded granites is included in Fig. 9 to show their Palaeozoic age (Olierook *et al.* 2020). The metasediments of the Nathorst Land Group on Wollaston Forland are thus comparable to the studied sediments, except that the metasediments contain a higher proportion of Mesoproterozoic zircons and no significant age populations in the 2.0–1.8 Ga interval.

The Meso–Neoproterozoic metasediments of the Krummedal supracrustal sequence and Smallefjord sequence have dominant zircon age populations of late Palaeoproterozoic age and additionally contain Mesoproterozoic, early Neoproterozoic and Palaeozoic populations (Strachan *et al.* 1995; Watt *et al.* 2000; Leslie & Nutman 2003). Thus, they are lacking 2.0–1.8 Ga age populations but otherwise resemble the age distributions of the studied sediments rather well. Archaean and Palaeoproterozoic crystalline basement complexes of the East Greenland Caledonides have age populations of 2.9–2.5 and 2.0–1.7 Ga (Kalsbeek *et al.* 1993; Thrane 2002; Elvevold *et al.* 2003). These are comparable to the oldest age populations found in the studied sediments, although the proportion of Palaeoproterozoic ages relative to Archaean ages is higher in the sediments than in the basement complexes.

Comparison between the samples analysed in this study and other sediments and possible sediment sources is made by multivariate statistical analysis by multidimensional scaling (MDS) visualised in an MDS diagram (Fig. 10). Here, similarities between samples are highlighted by solid lines revealing their proximity in Kolmogorov–Smirnov space, whereas dashed lines show smaller similarities. The sediments from this study have largest similarities to other Upper Jurassic and



**Fig. 10** Multidimensional scaling (MDS) diagram of zircon U-Pb age data. Plotted using Kolmogorov-Smirnov (K-S) dissimilarity (Vermeesch *et al.* 2016). The nearest neighbours in K-S space are shown by solid lines and the second nearest by dashed lines. See Fig. 10 for sample information.

Lower Cretaceous sediments, though some of these are as far away as Jameson Land. The largest differences are found between the end members comprising the Archaean–Palaeoproterozoic rocks and the Meso–Neoproterozoic metasediments, indicating that a mixture of these is necessary to explain the range of ages encountered in the sediments.

## 5.2 Sediment transport

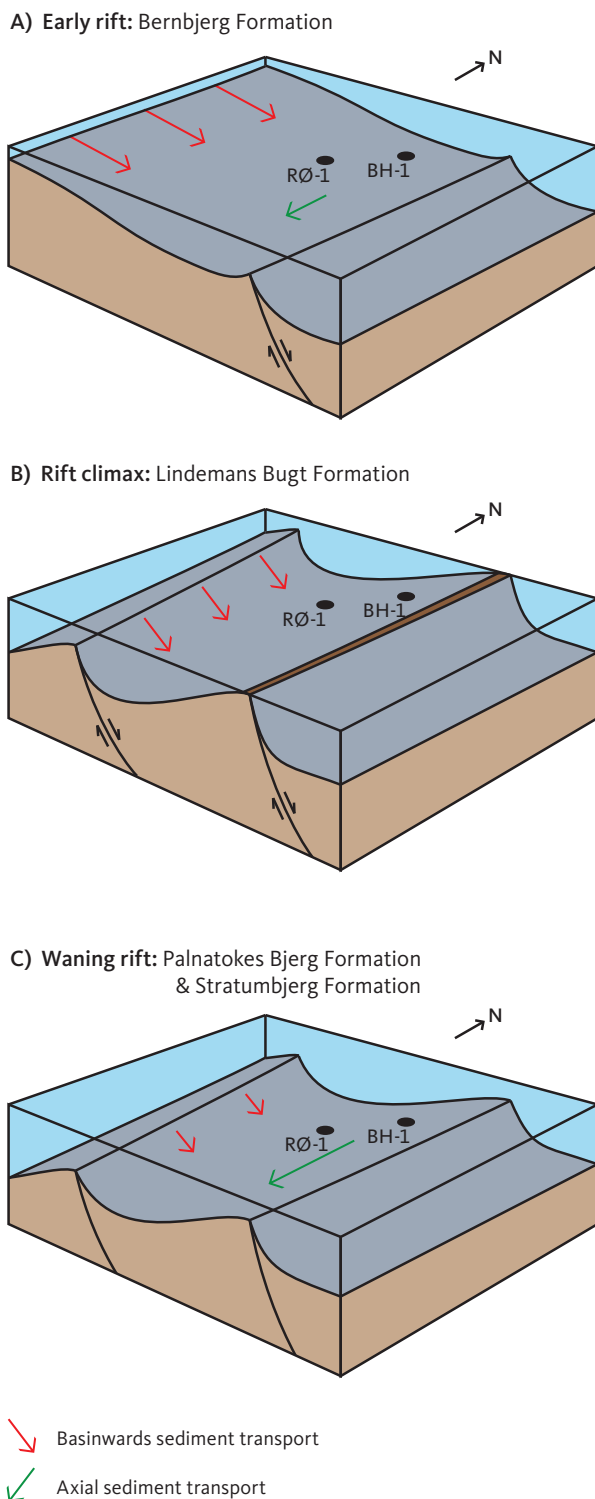
An overall north–south change in provenance in the upper Palaeozoic to Mesozoic succession in East Greenland is evident in the concentration of Palaeoproterozoic zircons in sediments on Wollaston Forland and Hold with Hope compared with sediments farther south, which contain a higher proportion of Mesoproterozoic zircons (Fig. 9). In particular, 2.0–1.8 Ga zircons are abundant in the central and northern parts of East Greenland in Triassic, Jurassic and Cretaceous sediments (Fonneland *et al.* 2004; Sláma *et al.* 2011; this study). This implies that there must be pronounced differences between either age or extent, or both, of the various sediment source rocks in the northern versus southern parts of the Caledonides. Factors such as zircon fertility, sediment routing, recycling and methodological bias may also affect the provenance signal (e.g. Dröllner *et al.* 2021).

The primary source of the Upper Jurassic – Lower Cretaceous sediments on Wollaston Forland comprised the crystalline rocks of the East Greenland Caledonides or their derived sediments, or both. The Archaean and Palaeoproterozoic ages of the basement in Payer Land (Elvevold *et al.* 2003) match the oldest age populations of the studied sediments, so they may have been supplied

from the crystalline complexes present west of Wollaston Forland (Fig. 1). An additional sediment source is necessary to account for the late Palaeoproterozoic peak age of 1.65–1.63 Ga and the range of Mesoproterozoic ages present in the studied sediments (Fig. 9), so this input must originate from erosion of Meso–Neoproterozoic metasediments or Palaeozoic sediments, or both.

The peak zircon age of 1.66–1.63 Ga is evident and often dominant in the sediments and metasediments of the East Greenland Caledonides (Fig. 9), except for the Lyell Land Group in which the peak ages are restricted to 1.5 and 1.1 Ga (Sláma *et al.* 2011). Peak ages of 1.5 and 1.1 Ga are also present in the Krummedal supracrustal sequence, the Nathorst Land Group and younger sediments such as the Devonian and Carboniferous, but are not pronounced in the studied sediments. However, these peak ages are distinct in the Upper Jurassic sediments on Jameson Land that are age-equivalent to the Bernbjerg Formation (Fig. 9). This is due to the lower proportion of Mesoproterozoic zircon ages in the northern part of the East Greenland Caledonides and in the studied sediments, which makes the individual age populations in this interval less distinct. Some change in the drainage pattern must have occurred between the Kimmeridgian – early Volgian and the Albian, since the distinct Archaean and 1.97 Ga populations in the Bernbjerg Formation are not evident in the Stratumbjerg Formation where a 1.88 Ga population is dominant, as observed in Aptian sediments on northern Hold with Hope. Ages corresponding to these populations are present in different crystalline basement complexes (Fig. 9).

Zircon age distributions of the Bernbjerg, Lindemans Bugt, Palnatokes Bjerg and Stratumbjerg Formations from western Wollaston Forland are comparable to each other (Barham *et al.* 2020) and broadly comparable to the new results from northern Wollaston Forland (Fig. 9). However, the pronounced peak age of 1.97 Ga in the three samples from the Bernbjerg Formation in northern Wollaston Forland is not present in samples from the west. Likewise, Caledonian zircons are also virtually absent in the west in contrast to the northern part of Wollaston Forland. Thus, although much of the sediment on northern Wollaston Forland has been produced from reworking of sediment from western Wollaston Forland (Fig. 11), there must also have been an additional source that supplied sediment to the half-graben in which the Rødryggen-1 and Brorson Halvø-1 boreholes are situated. This additional sediment was probably supplied by axial transport from the north in accordance with the general depositional pattern in the Late Jurassic (Surlyk 2003). This is compatible with the abundance of Palaeoproterozoic basement to the north



**Fig. 11** Inferred structural setting of northern Wollaston Forland in Late Jurassic to Early Cretaceous time when submarine deposition of mudstones took place during (A) early rifting, (B) rifting climax and (C) waning rifting in west (not waning in east, i.e. Falskebugt Member). Locations of the Rødryggen-1 (RØ-1) and Brorson Halvø-1 (BH-1) boreholes are shown as well as sediment transport directions.

and the presence of Caledonian granites in this area, though it is unknown if these granites were exposed in the Mesozoic.

Changes in sediment composition are also evident in the clay mineral composition where chlorite and

vermiculite were added upwards in the succession (Figs 3, 4). Another difference between the Bernbjerg Formation and the younger deposits is evident in the zircon age distributions from northern Wollaston Forland where the Stratumbjerg Formation lacks the Archaean and 1.97 Ga age populations that are present in the Bernbjerg Formation (Fig. 9). Thus, the rifting activity probably changed the erosional pattern resulting in altered sediment transport pathways. The kaolinite that is overgrown by authigenic quartz in the mudstones must comprise detrital kaolinite since they do not occur in well-defined booklets (Fig. 7C). The climate was humid subtropical at the time of deposition (Surlyk 2003), so kaolinite is the most likely clay mineral to have formed in the hinterland (Rateev *et al.* 2008), which explains its abundance in the mudstones. The presence of detrital kaolinite with preserved euhedral shapes points to a short transport distance from source area to place of deposition. This agrees with the interpreted proximity to the deltaic coast of North-East Greenland (Hovikoski *et al.* 2023b) with high mountains consisting of readily erodible material in the immediate hinterland (Henriksen & Higgins 2008).

### 5.3 Tectonic regime

Comparing the mineralogy of the carbonate-cemented mudstones with uncemented mudstones shows that the mudstones had similar initial mineralogical compositions, with the exception of the carbonate bioclasts, which represent the only additional component occurring in the cemented intervals (Figs 3, 4). Thus, in general, sediments with similar composition were supplied to the basin during deposition of the studied stratigraphic units, although the proportion between grains and clay minerals varies in relation to the grain size (Figs 3, 4). Other differences in the detrital mineralogy include the varying content of apatite clasts and the addition of vermiculite and chlorite to the clay mineral assemblages upwards in the succession. The variations in detrital mineralogy and grain size of the studied sediments are the results of (1) changing tectonic regime of the depositional setting that changed the sediment transport pathways and sea-bottom topography, and (2) rotational block faulting that caused increasing basin depth and sediment starvation up through the succession (Hovikoski *et al.* 2023a, this volume). Rifting also influenced the amount of deoxygenation and thereby the diagenetic evolution of the sediments as reflected in the varying amount of precipitated pyrite. The calcareous bioclast abundance is largest in transgressive intervals and in some condensed intervals as is also the case for apatite clasts.

The marine shelf setting of the Bernbjerg Formation with sediment supply from the deltaic coastline to the west (Fig. 11A) is reflected in the sandy component of the



mudstones with storm-wave influence in the lower part of the cored succession and in the presence of abundant silt and fine sand-sized quartz grains (Fig. 6C). Faulting intensified (Surlyk 2003), linked to the onset of coarse marine sedimentation proximally (Lindemans Bugt Formation). At the culmination of rotational block faulting, a fault was created west of the study area resulting in westwards tilting of the resulting basin (Fig. 11B; Hovikoski *et al.* 2023b). The submarine fault scarp west of this half-graben blocked sediment input from the mainland, but some sediment was supplied into the basin by gravity flows originating at the fault scarp. The fairly short distance to the fault scarp resulted in the input of some silt-sized detrital grains despite the relatively sediment-starved environment. Clasts of quartz, feldspar, mica and apatite (Fig. 6E) were supplied by mass flows in addition to the detrital clay minerals.

Vermiculite is absent in the Bernbjerg Formation in the Rødryggen-1 core but is found in all samples of the Lindemans Bugt and Palnatokes Bjerg Formations (Fig. 3). The cause of this change is not clear, but it may reflect the changed setting caused by block faulting whereby sediment supplied to the Rødryggen-1 drill site was sourced by the submarine fault scarp to the west during rift climax, and this input mixed with sediment supplied by axial transport during the waning rift phase (Fig. 11C). The high gamma-ray values of the Lindemans Bugt Formation in the Rødryggen-1 borehole (Fig. 3) are compatible with the fine-grained nature of the deposits in the centre of the half-graben where fine-crystalline vermiculite is dominant and coarse-crystalline kaolinite becomes less abundant, whereas the formation is only thinly preserved farther to the east in the Brorson Halvø-1 borehole (Fig. 4). Vermiculite does not occur in the succession in the Brorson Halvø-1 core, except for minor amounts in the uppermost sample from Stratumbjerg Formation. This is compatible with the larger distance to the submarine fault crest to the west that primarily fed vermiculite to the proximal part of the half-graben.

The Palnatokes Bjerg Formation is more sediment-starved than the Lindemans Bugt Formation due to transgression and waning of active rifting (Fig. 11C; Surlyk 2003). This is reflected in the high calcareous content suggestive of slow clastic deposition. The presence of occasional muddy sandstones, however, implies that gravity-flow processes were still operative. In the Brorson Halvø-1 core, chlorite occurs in the rift climax and waning rift samples, whereas it is only found in waning rift samples in the Rødryggen-1 core, and in smaller amounts (Figs 3, 4). This indicates that chlorite was supplied from the north-north-west by axial transport and deposited primarily in the distal part of the half-graben since the proximal part was mainly fed by the submarine

fault scarp to the west. The abundance of chlorite may have resulted from erosion of the Meso-Neoproterozoic metamorphic rocks north-west of Wollaston Forland that were exposed due to rift faulting, since chlorite often originates from such lithologies (Nielsen *et al.* 2015).

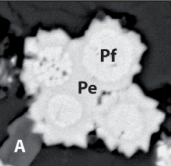
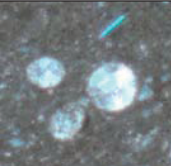
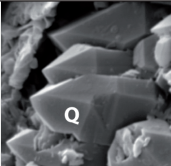
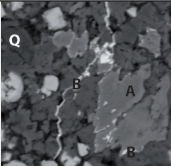

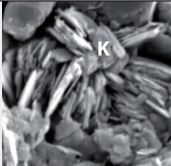
The provenance signature of the Stratumbjerg Formation near the Brorson Halvø-1 drill site is also indicative of a change in source area since the Archaean zircon age population is absent, in contrast to the Bernbjerg Formation (Fig. 9), which signifies a change in sediment source from the crystalline rocks to the west to the metamorphic and crystalline rocks to the north-west of the half-graben. This change is not evident in the zircon age distributions of the Palnatokes Bjerg and Lindemans Bugt Formations reported by Barham *et al.* (2020) because their samples were taken from localities within the proximal half-graben that were linked directly to the coastline.

## 5.4 Diagenetic evolution

Textural relationships in sediments of the Rødryggen-1 and Brorson Halvø-1 cores have been used to determine the diagenetic sequence. A diagenetic process scheme is established to highlight the relative importance of each process (Fig. 12), as discussed next. The sedimentary succession in the cores has poor reservoir quality since the few sandstone intervals are thin and muddy. The reservoir properties are poorest in the intervals with pervasive carbonate cementation. The formation of secondary porosity by partial dissolution of bioclasts and feldspars and by fracture formation has only had a minor influence on the total porosity. The permeability is only slightly affected by the dissolution process since it was restricted to local clasts. The open fractures, however, have presumably increased the permeability significantly.

### 5.4.1 Eogenetic processes

Pyrite framboids precipitated early in the sediments in association with bacterial sulphate reduction of organic matter (Fig. 7A). The membrane of organic matter in shells probably promoted early pyrite formation within many of the bioclasts (Fig. 8A). Euhedral pyrite formed only during the rift climax, corresponding primarily to the Lindemans Bugt Formation where the largest amounts of pyrite are found (Figs 3, 4, 5C, 7B). The small euhedral crystals suggest syngenetic formation of pyrite indicating that the chemocline moved above the sediment-water interface and anoxic conditions may have prevailed during the rift climax phase (Tribouillard *et al.* 2006) or the crystals may have formed later diagenetically. Dysoxic conditions were dominant when the rifting was still at an initial stage during deposition of the Bernbjerg Formation, and when rifting was waning as seen by the increased bioturbation and low

<i>Diagenetic process</i>	<b>Sulphate reduction</b>	<b>Bioclast alteration</b>	<b>Smectite illitization</b>	<b>Carbonate transformation</b>	<b>Fracture formation</b>	<b>Meteoric water flushing</b>
<b>Diagenetic regime</b>	Eogenesis	Eogenesis	Mesogenesis	Mesogenesis	Telogenesis	Telogenesis
<b>Temperature</b>	depositional	depositional	>80°C	80–100°C	<65°C	<50°C
<b>Dissolution</b>	organic matter, Fe-minerals	bioclasts, carbonate ooze	smectite, K-feldspar	dolomite, smectite	bulk mudstone	feldspar, mica
<b>Precipitation</b>	pyrite	calcite, dolomite	illite, quartz	ankerite, barite	opal, dolomite	kaolinite
<b>Porosity</b>	decreased	decreased	decreased	decreased	increased slightly	increased slightly
<b>Permeability</b>	decreased	decreased	decreased	decreased	increased	decreased slightly
<b>Requirements</b>	S from seawater	Mg from seawater	detrital smectite	Ba from initial seawater	source of water	supply of meteoric water
<b>Morphology</b>						

**Fig. 12** Diagenetic process scheme of the authigenic changes that have occurred in the Rødryggen-1 and Brorson Halvø-1 successions. See Section 5.4 for explanation.

pyrite content of the Palnatokes Bjerg and Stratumbjerg Formations. During sulphidic bottom-water conditions, the reactivity and abundance of Fe minerals control the amount of pyrite that can form, whereas pyrite formation is controlled by the reactivity and abundance of organic matter during oxygenated bottom-water conditions (Berner 1985). Thus, the low amounts (0–1%) of total organic carbon (TOC) present in the Palnatokes Bjerg and Stratumbjerg Formations largely precluded pyrite precipitation, whereas higher TOC (2–6%) in the Bernbjerg and Lindemans Bugt Formations (Bojesen-Koefoed *et al.* 2023b, this volume) will have favoured this process.

The calcite and dolomite cements probably formed shortly after deposition. The sparry carbonate cement within calpionellids in Bernbjerg and Lindemans Bugt Formations must have formed early after deposition since the calpionellids have not been deformed by mechanical compaction (Fig. 8A, B). The presence of bioclasts is important for the precipitation of dolomite and ankerite (e.g. Hendry *et al.* 2000; Burns *et al.* 2005) since they act both as nucleation sites for the crystals and as a source of carbonate. The Palnatokes Bjerg Formation was sediment-starved so pelagic lime mud formed a significant component of the sediment that accumulated on the sea floor, and the pelagic carbonate resulted in micritic calcite matrix (Fig. 7F).

In the Bernbjerg and Lindemans Bugt Formations, the laminated mudstones signify reducing conditions during deposition as also reflected in the relatively

high content of organic matter. In the Palnatokes Bjerg Formation, the bioturbation intensity reveals more oxygenated depositional conditions, and many of the bioclasts were preserved in this formation (Figs 8C, D). Partial dissolution of calpionellids and other bioclasts in the Bernbjerg and Lindemans Bugt Formations resulted in carbonate-cemented layers with a large bioclast content, caused by a primary heterogeneity (Fig. 7E). These layers possibly represent bioclast concentrations produced by reworking at discrete flooding surfaces (e.g. Burns *et al.* 2005). This is also suggested by the cemented mudstones that typically occur at the top of a few metres of upward-coarsening successions or in the finest grained intervals at the base of upward-coarsening cycles. The fewer cemented intervals in the Lindemans Bugt Formation in comparison to the Bernbjerg Formation (Fig. 3) are thus in accordance with the progressive deepening of the setting, where the influence of minor relative sea-level fluctuations decreased steadily.

### 5.4.2 Mesogenetic processes

The presence of authigenic mixed layer illite-smectite and illite in the studied mudstones indicates that illitisation of smectite has occurred, thereby providing silica and cations for other mineral reactions such as the formation of quartz and ankerite (Fig. 12). Significant illitisation may, however, be contradicted by the presence of K-feldspar in the investigated mudstones, as K-feldspar disappears in shales from most wells below 2.5 km in the northern North Sea due to the illitisation

of smectite (Pearson & Small 1988). If the deposited clay minerals were rich in illite, however, the pore fluids may not have been undersaturated with respect to potassium and consequently less aggressive towards K-feldspar during early diagenesis. Hence, K-feldspar may have survived until deep burial. The iron necessary to form ankerite may have been provided by smectite illitisation and it may have formed at the expense of dolomite cement. Barite is typically a late authigenic phase because the pore fluids need to be very concentrated before they contain sufficient Ba for barite formation. As expected, barite formed late in the studied sediments as seen by the crystal habit of barite as euhedral overgrowths (Fig. 7D), and the string-like occurrence of the precipitated barite identifies the transport route of the last pore fluid.

The diagenetic alteration of the mudstones is indicative of the maximum burial depths to which they have been exposed prior to structural inversion. The presence of quartz overgrowths shows that the sediments must have been exposed to temperatures of at least c. 80°C that is necessary for the growth onset and less than c. 100°C since they are thin and scattered (Bjørlykke & Jahren 2015). Precipitation of quartz in mudstones can be sourced by the smectite to illite transformation, which generally occurs at temperatures of 60–100°C (Thyberg *et al.* 2009) and is likely to have happened in the studied sediments. Barite precipitated after quartz and ankerite in the mudstones as the last mineral phase during deep burial, a process that has been found to occur at temperatures of 83–105°C in sandstones (Burley *et al.* 1989). Thus, the precipitation temperatures of the authigenic phases that formed at deepest burial correspond to maximum burial depths of c. 2.1–2.6 km assuming a surface temperature of 20°C and a palaeogeothermal gradient of 30°C/km (Japsen *et al.* 2021). This is less than the estimated uplift of c. 2.8 km based on thermochronological data from Upper Jurassic sediments from Jameson Land c. 450 km towards south-south-west, in which the diagenesis has progressed further (Green & Japsen 2018; Olivarius *et al.* 2018a).

#### 5.4.3 Telogenetic processes

The fracturing that has occurred in the sediments must have happened late during uplift since the thin fractures cross-cut the authigenic phases in the sediments. Fracturing is presumed to have accompanied exhumation and pressure release since cooling of the sediments was necessary to decrease their elasticity enough for fracturing (e.g. Gale *et al.* 2014). The fractures formed mainly in the cemented intervals because they had least elasticity. The late timing of the fracturing is also testified by the opal infill, which requires low temperatures of <65°C for precipitation (Weibel *et al.* 2010). The pore fluids must

have been oversaturated with silica in the beginning since opal often formed along the rim of the fractures (Fig. 8E). Formation of Fe-rich dolomite then took over in accordance with the expected composition of the pore fluid since the fractured mudstones are cemented with dolomite and ankerite. The pore fluid became depleted in Fe, so the last dolomite that precipitated was Fe-poor (Fig. 8F). The last fracturing episode happened so late during exhumation that no mineral phases were precipitated in the fractures, which thus contribute minor secondary porosity. However, it is difficult to differentiate natural open fractures, formed in the subsurface, from artefacts produced during drilling and drying of the core.

Introduction of meteoric water is a common mechanism for kaolinite formation (Bjørlykke 1998), as this process could not take place after deposition in the marine environment. The partially dissolved feldspar grains have not been deformed so the secondary porosity has been preserved (Fig. 6D), which indicates that the dissolution and kaolinisation of detrital phases may have happened late during the exhumation (Fig. 12). The fracturing that has occurred during late uplift may have caused a flow of meteoric water through the sediment that was sufficient for kaolinite formation. This may also explain why the latest generation of fractures is not cemented since the pore fluids had a low saturation.

### 5.5 Implications for sediment composition in the Norwegian–Greenland Seaway

The presence of Archaean zircon grains in the Norwegian Sea is often considered diagnostic of sediment supply from East Greenland since Archaean zircons are scarce in sediment eroded off the Fennoscandian Shield (e.g. Morton *et al.* 2008). Only a single Archaean zircon grain was retrieved from the sample from the Stratumbjerg Formation on Wollaston Forland (Fig. 9). However, the absence or scarcity of Archaean zircons cannot be considered unambiguous proof of a Fennoscandian source in the offshore sediments. This is particularly the case in sediment derived from the central or northern part of the East Greenland Caledonides where Palaeoproterozoic basement is most abundant, whereas Archaean basement is more abundant in the southern Caledonides (Thrane 2002). This is reflected in the geographical differences evident in the zircon age distributions of post-Caledonian sediments in East Greenland (Sláma *et al.* 2011; Olivarius *et al.* 2018b).

In sediments with an East Greenland source, the present results highlight how a high proportion of Mesoproterozoic and latest Palaeoproterozoic zircon ages testifies to a provenance from the southern East Greenland Caledonides, whereas a higher proportion of late Palaeoproterozoic

(2.0–1.7 Ga) ages is indicative of a more northern sediment source. This is reflected in the distribution of zircon age populations in sediments in the western part of the Norwegian Sea such as in the Upper Cretaceous – Paleocene succession (Fonneland *et al.* 2004; Morton *et al.* 2005).

Time-equivalent sediments in the Norwegian Sea have presumably experienced some of the same diagenetic reactions as the studied sediments, specifically, initial sulphate reduction causing pyrite precipitation, eogenetic bioclast alteration causing calcite-dolomite cementation, mesogenetic smectite illitisation and quartz precipitation and carbonate transformation into ankerite (Fig. 12).

## 6. Conclusions

This study illustrates that changes in mudstone composition can be induced by half-graben evolution and that the composition may also vary in relation to the position in the rift basin and the sea-bottom topography. This knowledge can be applied to predict variations in sediment composition in underexplored half-graben settings.

The diagenetic evolution includes processes related to the different diagenetic regimes that the mudstones have experienced. During early diagenesis, sulphate reduction caused pyrite formation, and bioclast alteration resulted in precipitation of calcite and dolomite. During burial diagenesis, illite and quartz formed due to smectite illitisation, and ankerite and barite precipitated because of carbonate transformation. During uplift, opal and dolomite precipitated in the earliest fractures, and kaolinite formed due to meteoric water flushing.

The provenance analysis of sand-rich intervals shows that the zircon age patterns of the studied sediments are most similar to other Upper Jurassic – Lower Cretaceous sandstones from East and North-East Greenland. This is revealed by MDS where it is evident that the Archaean–Palaeoproterozoic crystalline basement complexes and the Meso–Neoproterozoic metasediments comprise two end members, so their derived detritus must have been mixed to produce the Mesozoic sediments.

## Acknowledgements

Technical assistance by Helene Almind, Kirsten Fries, John Boserup, Fiorella F. Aguilera, Mojagan Alaei, Michael S. Nielsen and Jette Halskov is much appreciated. Valuable advice was provided by Emma Sheldon, Jon Ineson, Henrik Vosgerau, Holger Lindgreen and Tonci Balic-Zunic. The authors would like to thank the reviewers Chris Kirkland and Kevin Taylor for insightful comments that helped improve the manuscript.

## Additional information

### Funding statement

Funding for drilling of the Rødryggen-1 and Brorson Halvø-1 boreholes and studies of the cores was provided by a consortium of oil

companies and the Geological Survey of Denmark and Greenland (GEUS).

### Author contributions

MO: wrote the manuscript in cooperation with the other authors. MO, AK, RW: performed the mineralogical and petrographic work. TK: processed the radiometric analyses. JH: carried out the sedimentological work.

### Competing interests

None.

### Additional files:

The full table of zircon U-Pb data is provided as Supplementary File S1, available at <https://doi.org/10.22008/FK2/KELOA6>.

## References

- Alsen, P., Piasecki, S., Nøhr-Hansen, H., Pauly, S., Sheldon, E. & Hovikoski, J. 2023: Stratigraphy of the Upper Jurassic to lowermost Cretaceous in the Rødryggen-1 and Brorson Halvø-1 boreholes, Wollaston Forland, North-East Greenland. *GEUS Bulletin* **55**, 8342 (this volume). <https://doi.org/10.34194/geusb.v55.8342>
- Barham, M., Kirkland, C.L., Hovikoski, J., Alsen, P., Hollis, J. & Tyrrell, S. 2020: Reduce or recycle? Revealing source to sink links through integrated zircon–feldspar provenance fingerprinting. *Sedimentology* **68**, 531–556. <https://doi.org/10.1111/sed.12790>
- Berner, R.A. 1985: Sulphate reduction, organic matter decomposition and pyrite formation. Royal Society of London, Series A **315**, 25–38. <https://doi.org/10.1098/rsta.1985.0027>
- Bjerager, M. *et al.* 2020: Cretaceous lithostratigraphy of North-East Greenland. *Bulletin of the Geological Society of Denmark* **68**, 37–93. <https://doi.org/10.37570/bgsd-2020-68-04>
- Bjørlykke, K. 1998: Clay mineral diagenesis in sedimentary basins – a key to the prediction of rock properties. Examples from the North Sea Basin. *Clay Minerals* **33**, 15–34. <https://doi.org/10.1180/claymin.1998.033.1.03>
- Bjørlykke, K. & Jahren, J. 2015: Sandstones and Sandstone Reservoirs. In: Bjørlykke, K. (ed.): *Petroleum Geoscience: From Sedimentary Environments to Rock Physics* 119–149. Berlin, Heidelberg: Springer. [https://doi.org/10.1007/978-3-642-34132-8\\_4](https://doi.org/10.1007/978-3-642-34132-8_4)
- Bojesen-Koefoed, J.A., Alsen, P., Bjerager, M., Hovikoski, J., Ineson, J.R., Johannessen, P.N., Olivarius, M., Piasecki, S. & Vosgerau, H. 2023a: The Rødryggen-1 and Brorson Halvø-1 fully cored boreholes (Upper Jurassic – Lower Cretaceous), Wollaston Forland, North-East Greenland – an introduction. *GEUS Bulletin* **55**, 8350 (this volume). <https://doi.org/10.34194/geusb.v55.8350>
- Bojesen-Koefoed, J.A., Alsen, P., Bjerager, M., Hovikoski, J., Johannessen, P.N., Nøhr-Hansen, H., Petersen, H.I., Piasecki, S. & Vosgerau, H. 2023b: Organic geochemistry of an Upper Jurassic – Lower Cretaceous mudstone succession in a narrow graben setting, Wollaston Forland Basin, North-East Greenland. *GEUS Bulletin* **55**, 8320 (this volume). <https://doi.org/10.34194/geusb.v55.8320>
- Burley, S.D., Mullis, J. & Matter, A. 1989: Timing diagenesis in the Tartan reservoir (UK North Sea): Constraints from combined cathodoluminescence microscopy and fluid inclusion studies. *Marine and Petroleum Geology* **6**, 98–120. [https://doi.org/10.1016/0264-8172\(89\)90014-7](https://doi.org/10.1016/0264-8172(89)90014-7)
- Burns, F.E., Burley, S.D., Gawthorpe, R.L. & Pollard, J.E. 2005: Diagenetic signatures of stratal surfaces in the Upper Jurassic Fulmar Formation, Central North Sea, UKCS. *Sedimentology* **52**, 1155–1185. <https://doi.org/10.1111/j.1365-3091.2005.00729.x>
- Dhuime, B., Bosch, D., Bruguière, O., Caby, R. & Pourtales, S. 2007: Age, provenance and post-deposition metamorphic overprint of detrital zircons from the Nathorst Land group (NE Greenland) – A LA-ICP-MS and SIMS study. *Precambrian Research* **155**, 24–46. <https://doi.org/10.1016/j.precamres.2007.01.002>
- Dröllner, M., Barham, M., Kirkland, C.L. & Ware, B. 2021: Every zircon deserves a date: Selection bias in detrital geochronology. *Geological Magazine* **158**, 1135–1142. <https://doi.org/10.1017/S0016756821000145>
- Elvevold, S., Thrane, K. & Gilotti, J.A. 2003: Metamorphic history of high-pressure granulites in Payer Land, Greenland

- Caledonides. *Journal of Metamorphic Geology* **21**, 49–63. <https://doi.org/10.1046/j.1525-1314.2003.00419.x>
- Fonneland, H.C., Lien, T., Martinsen, O.J., Pedersen, R.B. & Košler, J. 2004: Detrital zircon ages: A key to understanding the deposition of deep marine sandstones in the Norwegian Sea. *Sedimentary Geology* **164**, 147–159. <https://doi.org/10.1016/j.sedgeo.2003.09.005>
- Gale, J.F.W., Laubach, S.E., Olson, J.E., Eichhubl, P. & Fall, A. 2014: Natural fractures in shale: A review and new observations. *AAPG Bulletin* **98**, 2165–2216. <https://doi.org/10.1306/08121413151>
- Gawthorpe, R.L. & Leeder, M.R. 2000: Tectono-sedimentary evolution of active extensional basins. *Basin Research* **12**, 195–218. <https://doi.org/10.1111/j.1365-2117.2000.00121.x>
- Gilotti, J.A., Jones, K.A. & Elvevold, S. 2008: Caledonian metamorphic patterns in Greenland. *Geological Society of America Memoir* **202**, 201–225. [https://doi.org/10.1130/2008.1202\(08\)](https://doi.org/10.1130/2008.1202(08))
- Green, P.F. & Japsen, P. 2018: Burial and exhumation history of the Jameson Land Basin, East Greenland, estimated from thermochronological data from the Blokelv-1 core. *Geological Survey of Denmark and Greenland Bulletin* **42**, 133–147. <https://doi.org/10.34194/geusb.v42.4324>
- Hendry, J.P., Wilkinson, M., Fallick, A.E. & Haszeldine, R.S. 2000: Ankerite cementation in deeply buried Jurassic sandstone reservoirs of the Central North Sea. *Journal of Sedimentary Research* **70**, 227–239. <https://doi.org/10.1306/2DC4090D-0E47-11D7-8643000102C1865D>
- Henriksen, N. & Higgins, A.K. 2008: Geological research and mapping in the Caledonian orogen of East Greenland, 70°N–82°N. In: Higgins, A.K. *et al.* (eds): *The Greenland Caledonides: Evolution of the North-east Margin of Laurentia*. *Geological Society of America Memoirs* **202**, 1–27.
- Henriksen, N., Higgins, A.K., Gilotti, J.A. & Smith, M.P. 2008: Introduction – The Caledonides of Greenland. *The Geological Society of America, Memoir* **202**, v–xv. [https://doi.org/10.1130/2008.1202\(00\)](https://doi.org/10.1130/2008.1202(00))
- Henstra, G.A. *et al.* 2016: Depositional processes and stratigraphic architecture within a coarse-grained rift-margin turbidite system: The Wollaston Forland Group, east Greenland. *Marine and Petroleum Geology* **76**, 187–209. <https://doi.org/10.1016/j.marpetgeo.2016.05.018>
- Higgins, A.K. *et al.* 2004: The foreland-propagating thrust architecture of the East Greenland Caledonides 72°–75°N. *Journal of the Geological Society* **161**, 1009–1026. <https://doi.org/10.1144/0016-764903-141>
- Hillier, S. 2000: Accurate quantitative analysis of clay and other minerals in sandstones by XRD: comparison of a Rietveld and a reference intensity ratio (RIR) method and the importance of sample preparation. *Clay Minerals* **35**, 291–302. <https://doi.org/10.1180/000985500546666>
- Hovikoski, J., Uchman, A., Alsen, P. & Ineson, J. 2018: Ichonological and sedimentological characteristics of submarine fan-delta deposits in a half-graben, Lower Cretaceous Palnatokes Bjerg Formation, NE Greenland. *Ichnos* **26**(1), 28–57. <https://doi.org/10.1080/10420940.2017.1396981>
- Hovikoski, J., Ineson, J.R., Olivarius, M., Bojesen-Koefoed, J.A., Piasecki, S. & Alsen, P. 2023a: Upper Jurassic – Lower Cretaceous of eastern Wollaston Forland, North-East Greenland: a distal marine record of an evolving rift. *GEUS Bulletin* **55**, 8349 (this volume). <https://doi.org/10.34194/geusb.v55.8349>
- Hovikoski, J. *et al.* 2023b: Late Jurassic – Early Cretaceous marine deoxygenation in NE Greenland. *Journal of the Geological Society* **180**, jgs2022–058. <https://doi.org/10.1144/jgs2022-058>
- Jackson, S.E., Pearson, N.J., Griffin, W.L. & Belousova, E.A. 2004: The application of laser ablation-inductively coupled plasma-mass spectrometry to in situ U–Pb zircon geochronology. *Chemical Geology* **211**, 47–69. <https://doi.org/10.1016/j.chemgeo.2004.06.017>
- Japsen, P., Green, P.F., Bonow, J.M., Bjerager, M. & Hopper, J.R. 2021: Episodic burial and exhumation in North-East Greenland before and after opening of the North-East Atlantic. *GEUS Bulletin* **45**(2), 5299. <https://doi.org/10.34194/geusb.v45.5299>
- Kalsbeek, F., Nutman, A.P. & Taylor, P.N. 1993: Palaeoproterozoic basement province in the Caledonian fold belt of North-East Greenland. *Precambrian Research* **63**, 163–178. [https://doi.org/10.1016/0301-9268\(93\)90010-Y](https://doi.org/10.1016/0301-9268(93)90010-Y)
- Kalsbeek, F., Thrane, K., Nutman, A.P. & Jepsen, H.F. 2000: Late Mesoproterozoic to early Neoproterozoic history of the East Greenland Caledonides: Evidence for Grenvillian orogenesis? *Journal of the Geological Society (London)* **157**, 1215–1225. <https://doi.org/10.1144/jgs.157.6.1215>
- Kalsbeek, F., Jepsen, H.F. & Nutman, A.P. 2001: From source migmatites to plutons: Tracking the origin of ca. 435 Ma S-type granites in the East Greenland Caledonian orogen. *Lithos* **57**, 1–21. [https://doi.org/10.1016/S0024-4937\(00\)00071-2](https://doi.org/10.1016/S0024-4937(00)00071-2)
- Kalsbeek, F., Thrane, K., Higgins, A.K., Jepsen, H.F., Leslie, A.G., Nutman, A.P. & Frei, R. 2008a: Polyorogenic history of the East Greenland Caledonides. *Geological Society of America Memoir* **202**, 55–72.
- Kalsbeek, F., Higgins, A.K., Jepsen, H.F., Frei, R. & Nutman, A.P. 2008b: Granites and granites in the East Greenland Caledonides. *Geological Society of America Memoir* **202**, 227–249. [https://doi.org/10.1130/2008.1202\(09\)](https://doi.org/10.1130/2008.1202(09))
- Langrock, U., Stein, R., Lipinski, M. & Brumsack, H.-J. 2003: Late Jurassic to Early Cretaceous black shale formation and paleoenvironment in high northern latitudes: Examples from the Norwegian-Greenland Seaway. *Paleoceanography* **18**, 1074. <https://doi.org/10.1029/2002PA000867>
- Larsen, P.-H., Olsen, H. & Clack, J.A. 2008: The Devonian basin in East Greenland – Review of basin evolution and vertebrate assemblages. *Geological Society of America Memoir* **202**, 273–292. [https://doi.org/10.1130/2008.1202\(11\)](https://doi.org/10.1130/2008.1202(11))
- Leslie, A.G. & Nutman, A.P. 2003: Evidence for Neoproterozoic orogenesis and early high temperature Scandian deformation events in the southern East Greenland Caledonides. *Geological Magazine* **140**, 309–333.
- McCusker, L.B., Von Dreele, R.B., Cox, D.E., Louer, D. & Scardi, P. 1999: Rietveld refinement guidelines. *Journal of Applied Crystallography* **32**, 36–50. <https://doi.org/10.1107/S0021889898009856>
- McKerrow, W.S., Mac Niocaill, C. & Dewey, J.F. 2000: The Caledonian Orogeny redefined. *Journal of the Geological Society (London)* **157**, 1149–1154. <https://doi.org/10.1144/jgs.157.6.1149>
- Morton, A.C., Whitham, A.G. & Fanning, C.M. 2005: Provenance of Late Cretaceous to Paleocene submarine fan sandstones in the Norwegian Sea: Integration of heavy mineral, mineral chemical and zircon age data. *Sedimentary Geology* **182**, 3–28. <https://doi.org/10.1016/j.sedgeo.2005.08.007>
- Morton, A., Fanning, M. & Milner, P. 2008: Provenance characteristics of Scandinavian basement terrains: Constraints from detrital zircon ages in modern river sediments. *Sedimentary Geology* **210**, 61–85.
- Mutterlose, J. *et al.* 2003: The Greenland-Norwegian Seaway: A key area for understanding Late Jurassic to Early Cretaceous paleoenvironments. *Paleoceanography* **18**, 1010. <https://doi.org/10.1029/2001PA000625>
- Nielsen, O.B., Rasmussen, E.S. & Thyberg, B.I. 2015: Distribution of clay minerals in the northern North Sea Basin during the Paleogene and Neogene: A result of source-area geology and sorting processes. *Journal of Sedimentary Research* **85**, 562–581. <https://doi.org/10.2110/jsr.2015.40>
- Nøhr-Hansen, H., Piasecki, S. & Alsen, P. 2020: A Cretaceous dinoflagellate cyst zonation for NE Greenland. *Geological Magazine* **157**, 1658–1692. <https://doi.org/10.1017/S0016756819001043>
- Olierook, H.K.H., Barham, M., Kirkland, C.L., Hollis, J. & Vass, A. 2020: Zircon fingerprint of the Neoproterozoic North Atlantic: Perspectives from East Greenland. *Precambrian Research* **342**, 105653. <https://doi.org/10.1016/j.precamres.2020.105653>
- Olivarius, M., Weibel, R., Schovsbo, N.H., Olsen, D. & Kjølner, C. 2018a: Diagenesis of Upper Jurassic sandstones of the Blokelv-1 core in the Jameson Land Basin, East Greenland. *Geological Survey of Denmark and Greenland Bulletin* **42**, 65–84. <https://doi.org/10.34194/geusb.v42.4310>
- Olivarius, M., Bjerager, M., Keulen, N., Knudsen, C. & Kokfelt, T.F. 2018b: Provenance of basinal sandstones in the Upper Jurassic Hareelv Formation, Jameson Land Basin, East Greenland. *Geological Survey of Denmark and Greenland Bulletin* **42**, 115–126. <https://doi.org/10.34194/geusb.v42.4317>
- Pearson, M.J. & Small, J.S. 1988: Illite-smectite diagenesis and palaeotemperatures in northern North Sea Quaternary to Mesozoic shale sequences. *Clay Minerals* **23**, 109–132. <https://doi.org/10.1180/claymin.1988.023.2.01>
- Piasecki, S., Bojesen-Koefoed, J.A. & Alsen, P. 2020: Geology of the Lower Cretaceous in the Falkebjerg area, Wollaston Forland, northern East Greenland. *Bulletin of the Geological Society of Denmark* **68**, 155–170.

- Rateev, M.A., Sadchikova, T.A. & Shabrova, V.P. 2008: Clay minerals in recent sediments of the world ocean and their relation to types of lithogenesis. *Lithology and Mineral Resources* **43**, 125–135. <https://doi.org/10.1134/S002449020802003X>
- Rietveld, H.M. 1969: A profile refinement method for nuclear and magnetic structures. *Journal of Applied Crystallography* **2**, 65–71. <https://doi.org/10.1107/S0021889869006558>
- Rogov, M.A., Shchepetova, E.V. & Zakharov, V.A. 2020: Late Jurassic – Earliest Cretaceous prolonged shelf dysoxic-anoxic event and its possible causes. *Geological Magazine* **157**, 1622–1642. <https://doi.org/10.1017/S001675682000076X>
- Sambridge, M. & Lambert, D.D. 1997: Propagating errors in decay equations: Examples from the Re-Os isotopic system. *Geochimica et Cosmochimica Acta* **61**, 3019–3024.
- Sláma, J. & Košler, J. 2012: Effects of sampling and mineral separation on accuracy of detrital zircon studies. *Geochemistry, Geophysics, Geosystems* **13**, Q05007. <https://doi.org/10.1029/2012GC004106>
- Sláma, J. *et al.* 2008: Plešovice zircon – A new natural reference material for U–Pb and Hf isotopic microanalysis. *Chemical Geology* **249**, 1–35. <https://doi.org/10.1016/j.chemgeo.2007.11.005>
- Sláma, J., Walderhaug, O., Fonneland, H., Kosler, J. & Pedersen, R.B. 2011: Provenance of Neoproterozoic to upper Cretaceous sedimentary rocks, eastern Greenland: Implications for recognizing the sources of sediments in the Norwegian Sea. *Sedimentary Geology* **238**, 254–267. <https://doi.org/10.1016/j.sedgeo.2011.04.018>
- Slater, C. & Cohen, L. 1962: A centrifugal particle size analyser. *Journal of Scientific Instrumentation* **39**, 614–617.
- Smith, M.P. & Rasmussen, J.A. 2008: Cambrian–Silurian development of the Laurentian margin of the Iapetus Ocean in Greenland and related areas. *Geological Society of America Memoir* **202**, 137–167. [https://doi.org/10.1130/2008.1202\(06\)](https://doi.org/10.1130/2008.1202(06))
- Stacey, J.S. & Kramers, J.D. 1975: Approximation of terrestrial lead isotope evolution by a two-stage model. *Earth and Planetary Science Letters* **26**, 207–221. [https://doi.org/10.1016/0012-821X\(75\)90088-6](https://doi.org/10.1016/0012-821X(75)90088-6)
- Stemmerik, L., Christensen, F.G., Piasecki, S., Jordt, B., Marcussen, C. & Nøhr-Hansen, H. 1992: Depositional history and petroleum geology of the Carboniferous to Cretaceous sediments in the northern part of East Greenland. Norwegian Petroleum Federation, Special Publication **2**, 67–87. <https://doi.org/10.1016/B978-0-444-88943-0.50009-5>
- Stemmerik, L., Clausen, O.R., Korstgård, J., Larsen, M., Piasecki, S., Seidler, L., Surlyk, F. & Therkelsen, J. 1997: Petroleum geological investigations in East Greenland: Project ‘Resources of the sedimentary basins of North and East Greenland’. *Geological Survey of Greenland Bulletin* **176**, 29–38. <https://doi.org/10.34194/ggub.v176.5058>
- Stoker, M.S. *et al.* 2017: An overview of the Upper Palaeozoic–Mesozoic stratigraphy of the NE Atlantic region. Geological Society, London, Special Publications **447**, 11–68. <https://doi.org/10.1144/SP447.2>
- Strachan, R.A., Nutman, A.P. & Friderichsen, J.D. 1995: SHRIMP U–Pb geochronology and metamorphic history of the Smallefjord sequence, NE Greenland Caledonides. *Journal of the Geological Society* **152**, 779–784.
- Surlyk, F. 1978: Submarine fan sedimentation along fault scarps on tilted fault blocks (Jurassic–Cretaceous boundary, East Greenland). *Geological Survey of Greenland Bulletin* **128**, 108 pp. <https://doi.org/10.34194/bullggu.v128.6670>
- Surlyk, F. 1984: Fan-delta to submarine fan conglomerates of the Volgian–Valanginian Wollaston Forland Group, East Greenland. *Canadian Society of Petroleum Geologists Memoir* **10**, 359–382.
- Surlyk, F. 1990: A Jurassic sea-level curve for East Greenland. *Palaeogeography, Palaeoclimatology, Palaeoecology* **78**, 71–85. [https://doi.org/10.1016/0031-0182\(90\)90205-L](https://doi.org/10.1016/0031-0182(90)90205-L)
- Surlyk, F. 2003: The Jurassic of East Greenland: A sedimentary record of thermal subsidence, onset and culmination of rifting. *Geological Survey of Denmark and Greenland Bulletin* **1**, 659–722. <https://doi.org/10.34194/geusb.v1.4674>
- Surlyk, F. & Korstgård, J. 2013: Crestal unconformities on an exposed Jurassic tilted fault block, Wollaston Forland, East Greenland as an analogue for buried hydrocarbon traps. *Marine and Petroleum Geology* **44**, 82–95. <https://doi.org/10.1016/j.marpetgeo.2013.03.009>
- Surlyk, F. *et al.* 2021: Jurassic stratigraphy of East Greenland. *GEUS Bulletin* **46**, 6521. <https://doi.org/10.34194/geusb.v46.6521>
- Thrane, K. 2002: Relationships between Archaean and Palaeoproterozoic crystalline basement complexes in the southern part of the East Greenland Caledonides: An ion microprobe study. *Precambrian Research* **113**, 19–42. [https://doi.org/10.1016/S0301-9268\(01\)00198-X](https://doi.org/10.1016/S0301-9268(01)00198-X)
- Thyberg, B., Jahren, J., Winje, T., Bjørlykke, K. & Faleide, J.I. 2009: From mud to shale: Rock stiffening by micro-quartz cementation. *First Break* **27**, 27–33. <https://doi.org/10.3997/1365-2397.2009003>
- Tribouvillard, N., Algeo, T.J., Lyons, T. & Riboulleau, A. 2006: Trace metals as paleoredox and paleoproductivity proxies: An update. *Chemical Geology* **232**, 12–32. <https://doi.org/10.1016/j.chemgeo.2006.02.012>
- Vermeesch, P. 2012: On the visualisation of detrital age distributions. *Chemical Geology* **312–313**, 190–194. <https://doi.org/10.1016/j.chemgeo.2012.04.021>
- Vermeesch, P., Resentini, A. & Garzanti, E. 2016: An R package for statistical provenance analysis. *Sedimentary Geology* **336**, 14–25. <https://doi.org/10.1016/j.sedgeo.2016.01.009>
- Watt, G.R., Kinny, P.D. & Friderichsen, J.D. 2000: U–Pb geochronology of Neoproterozoic and Caledonian tectonothermal events in the East Greenland Caledonides. *Journal of the Geological Society* **157**, 1031–1048. <https://doi.org/10.1144/jgs.157.5.1031>
- Weibel, R., Friis, H., Kazerouni, A.M., Svendsen, J.B., Stokkendal, J. & Poulsen, M.L.K. 2010: Development of early diagenetic silica and quartz morphologies. *Sedimentary Geology* **228**, 151–170. <https://doi.org/10.1016/j.sedgeo.2010.04.008>